Drone Systems and Applications

OPEN ACCESS | Research Article

Mathematical model and computer program development for online modeling of pulse jet engine working cycle, parameters, and characteristics

Alexander Khrulev and Valeriy Muntyan

International Motor Bureau, Nemishaeve, Kyiv region, Ukraine

Corresponding author: **Alexander Khrulev** (email: info@engine-expert.com)

Abstract

The work is devoted to the development of a mathematical model and a program for online modeling of the pulse jet engine working cycle and characteristics to assess the possibility of its use on unmanned aerial vehicles. The developed universal thermodynamic model describes the instantaneous change in pressure and temperature, taking into account the mixing of flows, combustion, and heat exchange in the combustion chamber of valved and valveless types of pulse jet engines, as well as the flows through the pipes and reed valves of various designs. Unlike the known works, a special online program, Pulsejet-Sim, for pulsejet modeling by a wide range of users has been developed for the first time, which is posted on a special website as a web-oriented software service that does not require downloading to the user's computer and allows for instant calculation using server resources and secure data cloud storage. Using the developed software, preliminary mathematical modeling of known samples of pulse jet engines was performed, which showed generally satisfactory qualitative and quantitative agreement of the modeling results (error less than 10%) with the available experimental data on thrust, specific fuel consumption, cycle frequency, and other parameters.

Key words: pulse jet engine, pulsejet modeling, valved, valveless, simulation, piston analogy model

Introduction

The pulse jet engine has played a significant role in aviation history, demonstrating the effectiveness of a simple and inexpensive military technology in its mass application (Schmidt 1957). However, not only advantages, but also serious pulsejet disadvantages were noted, namely, excessive noise, unmasking the aircraft, and significant vibrations transmitted from the engine to the aircraft structure (Gosslau 1957). In addition, the extremely high temperature of the engine walls, preventing its placement inside the aircraft fuselage (Diedrich 1948), significant fuel consumption, limiting flight range and duration (Sánchez 2022), as well as the limited service life of the intake valves due to the complex impact and temperature effects (Manganiello et al. 1945*b*) turned out to be the negative factors.

These disadvantages turned out to be almost insurmountable obstacles to the further development and distribution of pulse jet engines in aviation. As a result, the pulsejets turned out to be in demand for solving a very limited range of problems, mainly for attack unmanned aerial vehicles (UAVs) (Prisacariu 2022) of a relatively short range (up to several hundred kilometers) and for target drones (Globe Corporation 2025). At the same time, given the fact that the valve mechanism is a weak point of the classic valved pulse jet engine, many efforts were aimed at creating designs for valveless pulsejets (Lockwood 1963; Mittal 2025). However, in the overwhelming majority of cases, all these efforts were also not crowned with noticeable success, although some more or less successful examples of small-scale designs of valveless pulsejets are known (Newdick 2024).

In general, it can be noted that interest in the pulse jet engine has risen periodically over the past 80 years, in waves, which led to a revival and then a fading of interest in it. Today, some signs indicate that the topic of pulsejets has not been forgotten and may again be on the rise (Wave Engine Corp. 2025), although perhaps not too long, as it was in the past years (Fig. 1). Nevertheless, issues of research into pulsejets may again be on the agenda (Wikipedia 2025*c*).

And here the main problem arises. Although theoretical models of pulsejet workflow have been developed over many years, and even in large quantities, it remains unclear for what purpose these works were carried out. It is quite possible that the purpose of some works was to solve their own problems by individual scientists, write scientific articles, and satisfy their own ambitions and/or some other not entirely clear goals. But no theoretical models or calculation programs for pulsejet simulation suitable by users for practical use have been created over all these years.

Fig. 1. Some modern unmanned aerial vehicles with a pulse jet engine: (*a*) Scitor from Wave Engine Corporation, USA (Wave Engine Corp. 2025) and (*b*) Trembita from PARS, Ukraine (Wikipedia 2025*c*).

a b

Problem statement

An analysis of numerous sources shows that a significant proportion of the known works was not done for design purposes, not for creating real engines, and not so that everyone could use the developed calculation models to design new engines.

This situation is rather strange, because in general there is no shortage of theoretical models for pulsejet workflow—on the contrary, quite a lot of different models are known. Thus, the very first calculation model can be considered the model of one of the pulsejet founders Dr. Schulz-Grunow (Shultz-Grunow 1947); this is the famous method of characteristics (Wikipedia 2025*b*). This method has its supporters and is very popular, since it allows calculating the propagation of waves in a compressible medium, and this is exactly what is required when modeling a pulse jet engine. However, for some reason, no standard and user-friendly programs for pulsejet calculating based on the method of characteristics have been created in the 80 years of its popularity. At least, nothing is known about such programs so far.

A number of well-known scientific works are devoted to thermodynamic models of a pulsejet engine, including within the framework of the so-called "piston" analogy of gas motion in a resonant exhaust pipe (Khrulev 2023*a*), when the gas is considered as a kind of "liquid piston" (Anand et al. 2020). One of the founders of this method should be recognized as the Soviet scientist Prof. E.S. Shchetinkov (Schetinkov 1965), whose developments date back to the 40s of the last century. Incidentally, a similar principle was later adopted in the study of pulsejets by other scientists, including those at the University of Cincinnati (Anand et al. 2020). However, no theoretical models based on the "liquid piston" analogy, and even more so, ready-made calculation programs, have yet appeared that are practically useful for independent users. Methods are also known based on a one-dimensional representation of gas flow in a resonant pipe (Meng et al. 2015). And there are also methods built on the acoustic analogy of oscillations excited in a Helmholtz resonator (Van Heerbeek 2008). But it will be difficult to use these models for ordinary user if he solves to take advantages for developing his pulse jet engine.

A difficult situation arose also with the emergence and widespread introduction of 3D modeling into scientific practice. Having such a good tool, some scientists focused in their articles on obtaining the spatial distribution of gas parameters along the pulsejet pipe (Mohsen et al. 2021). Others hastened to concentrate their efforts on the features of modeling three-dimensional flow with chemical reactions of pulse combustion (Agarwal and Pitso 2020). Thirds began to develop their own 3D models of the pulse jet engine, switching their attention, among other things, to the spatial movements of the valve petals with transverse oscillations (Gonzalez et al. 2017).

In result, of over 80 years, the pulse jet engine has been studied very well, thousands of articles have been written, hundreds of models for its calculation have been invented, and even books have been published (Migalin et al. 2014). But for some reason, up to now, a formula for this engine's thrust is still unknown. In addition, the vast majority of pulsejet works do not study its main operational characteristic as an aircraft engine—altitude and speed. Meanwhile, this is one of the main questions of the jet engine theory. It is with this that the study of aircraft engines begins, and the magnitude of thrust is not only the main parameter (Rolls-Royce 1996), but should also be the goal of any engine study.

Therefore, it is quite natural that all known and very deep studies are united by one and the same result: no standard programs for modeling a pulse jet engine and its characteristics suitable for wide practical application have been created after such efforts. The user was once again offered to actually buy an expensive 3D modeling program himself, figure it out himself, having undergone appropriate training, then create a model in this program himself, debug it, and only after that model his engine. In this case, it is necessary to repeat all the steps already performed by this or that scientist and described in his article. But it is simply not possible for an ordinary user to do all this.

And indeed, in most practical cases, it has already become traditional to begin the creation of a new sample of a pulse jet engine not with a study of the working process and not with the creation of theoretical models that allow calculating the parameters and altitude–speed characteristics for subsequent UAV's design, but with the help of some dimension calculators (Ahmadian 2014), with cutting steel sheets and welding pipes from them (Simpson 2004).

The described situation with the modeling of pulsejets is fundamentally different from what is observed in the field of modeling other types of aircraft engines. Thus, for many years, standard programs have been widely used for modeling piston internal combustion engines (Pearson et al. 2002), four of which are widely known. Similarly, for modeling gas turbine engines, there are also a number of standard programs (GasTurb 2023), and the program not only gives the parameters of the engine working process and altitude–speed characteristics, but also draws the appearance of the modeled engine. None of this has yet been created for pulsejets.

Summing up the review, it can be said that for many decades, a contradictory situation has been observed in pulsejet studies. On the one hand, there are the numerous examples of theoretical models, but a normal working model and program for simulating the pulse jet engine working cycle and characteristics, suitable for wide practical use, could not be created yet. And on the other hand, none of the known models are essentially operational due to the lack of ready-made programs, excessive complexity and/or cost, impossibility of acquisition, or for some other reason that prevents their wide use by an ordinary user.

This generally prevents not only understanding the working process of a pulse jet engine, but also a reliable assessment of the possibility and feasibility of its use on UAVs of various purposes.

The purpose and objectives of the study

According to the analysis performed, the purpose of the work is to create a mathematical model and a real program for simulating the working cycle and characteristics of a pulse jet engine, suitable for assessing the possibility of its use on UAVs and accessible to a wide range of specialists and ordinary users.

To achieve this goal, it was necessary to solve the following problems:

- Develop a model for describing the processes in the combustion chamber of a pulse jet engine.
- Develop a model for describing the processes of air and fuel intake into the combustion chamber, including through a reed valve for a valved engine.
- Develop a model of air and gas flow in the resonance pipe of a pulse jet engine and in the intake pipe of a valveless engine.
- Develop and debug the engine simulation program, and place it on a special websitefor access by a wide range of specialists and ordinary users.
- Perform mathematical modeling of engine samples, verify the model and program by comparing the results with known experimental data.

Materials and methods

The proposed model is based on the numerical solution of a system of homogeneous differential equations obtained from the equations of continuity, motion and energy by introducing some simplifying assumptions regarding the nature of the working process using experimental data on fuel combustion, friction, and heat transfer. The choice of this simplified representation of the processes, and not a 1D and, especially, a 3D model, is deliberately due to the need for a preliminary check of the idea of creating an online modeling program available to a wide range of users. However, after launching and debugging the program, further improvement of the model is possible in any way, including increasing the dimensionality of individual models included in the general algorithm, as is done in some programs for modeling internal combustion engines (Khrulev 2024).

The working process of a pulse jet engine (Fig. 2) can be represented as a process of forced oscillations of gas parameters (pressure, temperature, and speed) in the engine flow part with a pulsating nature of heat supply. Then the wavelength of these oscillations can be determined by the formula $\bar{\varphi} = \bar{a}/\overline{f}$, where $\bar{a}$ is the sound speed; $\bar{f}$ is the oscillation frequency.

Let L be some characteristic dimension, e.g., the length of the combustion chamber. If the oscillations have a sinusoidal shape, then by the ratio $\frac{L}{\varphi} = L\frac{\bar{f}}{\bar{a}}$ one can approximately determine how great the difference in parameters at different ends of the chamber is. Thus, for known designs of pulsejets (Simpson 2004; Anand et al. 2019*a*) this ratio is no more than 0.03–0.05. This means that if we assume that the pressure and temperature are the same at all points of the combustion chamber, the error will not exceed 3%–5%. Therefore, the spatial uniformity of the distribution of thermodynamic parameters of gas in the combustion chamber is the first assumption of the method. A consequence of this is the assumption of a volumetric form of combustion of the fuel–air mixture, which is generally confirmed by experimental data (Anand et al. 2019*b*).

If the same assumption is made for the resonance pipe as for the combustion chamber, the error will already be about 15% (if it is calculated as the average difference in the values of the sinusoidal function over a cycle in the section of 1/10 of the full cycle; the maximum difference near 0 is about 30%, the minimum difference near the maximum of function is about 2%). However, if such an assumption is not accepted, then the problem of non-stationary gas flow in the exhaust pipe becomes much more complicated even in a one-dimensional formulation. In order not to complicate the method at the preliminary stage, but to ensure acceptable accuracy, it is assumed that the instantaneous values of velocity, pressure, and temperature along the length of the pipe are constant (i.e., the gas in the pipe actually flows as an incompressible liquid), but a correction for compressibility can be introduced. Such a representation of the process is known and is called the “piston analogy” or “liquid piston” (Anand et al. 2019*a*; 2019*b*).

In addition, it should be noted that dimensionless complexes characterizing the working process of the engine under study can be of great importance for practice. To obtain such complexes, it is possible to write the equations describing the processes in dimensionless form. To do this, we should move on to dimensionless variables: pressure $p = \frac{\bar{p}}{\bar{p}_0}$, temperature $T = \frac{\bar{T}}{\bar{T}_0}$, velocity $v = \frac{\bar{v}}{\bar{v}_0}$, time $t = \bar{t}\frac{\bar{a}_0}{L}$, coordinate $x = \frac{\bar{x}}{L}$, where $\bar{p}_0$, $\bar{T}_0$ are the environment pressure and temper-

Fig. 2. Schematic diagram of a pulse jet engine: (*a*) valved, (*b*) valveless, 1—inlet device (inlet pipe), 2—fairing, 3—valve grid, 4—petal valve, 5—limiter, 6—combustion chamber, 7—nozzle, and 8—resonance pipe.

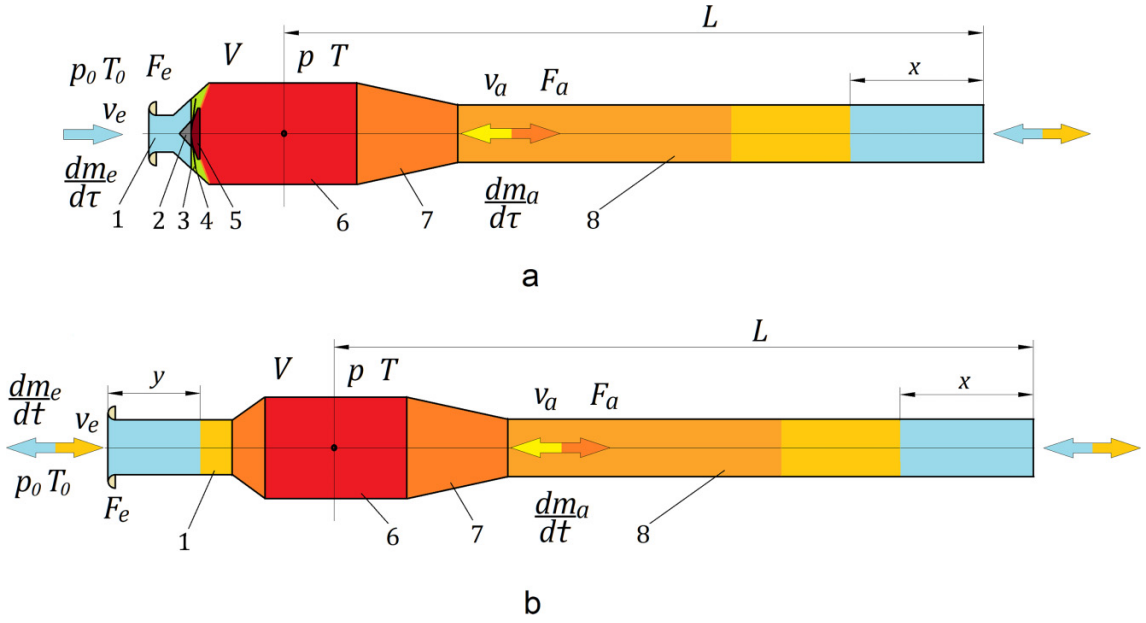

ature; $\bar{a}_0 = \sqrt{\gamma \bar{R}_0 \bar{T}_0}$ is the speed of sound in the environment; L is the characteristic size of the engine.

Some other quantities that may be needed later can be written in dimensionless form too: heat capacity of gas at constant pressure $C_p = \frac{\bar{C}_p}{\bar{C}_{p0}}$, gas constant $R = \frac{\bar{R}}{\bar{R}_0}$, gas density $\rho = \frac{\bar{\rho}}{\bar{\rho}_0}$, specific heat flux into the wall $q_w = \frac{\bar{q}_w}{\bar{\rho}_0 \bar{a}_0 \bar{C}_{p0} \bar{T}_0}$, fuel calorific value $H_u = \frac{H_u}{\bar{C}_{p0} \bar{T}_0}$, volumetric heat release rate $\frac{\mathrm{d}Q}{\mathrm{d}t} = \frac{\mathrm{d}\bar{Q}}{\mathrm{d}\bar{t}} \frac{L}{\bar{a}_0 \bar{C}_{p0} \bar{T}_0}$, rate of mass change (instantaneous mass flow rate) $\frac{\mathrm{d}m}{\mathrm{d}t} = \frac{\mathrm{d}\bar{m}_i / \mathrm{d}\bar{t}}{\bar{\rho}_0 \bar{a}_0 F}$.

The ambient pressure and temperature included in these expressions may vary with the flight altitude H of the aircraft. In addition, the ambient parameters are necessary for modeling the altitude–speed characteristics of the engine of the type under study. For this purpose, the following formulas of the international standard atmosphere are used in the model (Cavcar 2025)

$$\bar{p}_0 = 101325\left(1 - 0,0065H/\bar{T}_0\right)^{5,2561},$$
$$\bar{T}_0 = 288,15 - 0.00649H$$

The length from the center of combustion chamber to the edge of the resonance tube, L, is chosen as the characteristic size of the engine, since this value determines the length of the entire engine and, in addition, is important from the point of view of the stability of the operation and start-up of the pulsejet (Simpson 2004), as well as the thrust force.

Model for describing processes in the combustion chamber of a pulse jet engine

The basic principles of constructing thermodynamic models of engines and different similar units are set out by us in (Khrulev 2024); however, when applied to a pulsejet engine, the derivation of equations has its own peculiarities.

Let us consider the energy equation for the allocated volume of the combustion chamber in the form:

$$\bar{m}\mathrm{d}\bar{Q} = \mathrm{d}\bar{I} + V\mathrm{d}\bar{p}, \tag{1}$$

where $\mathrm{d}\bar{Q}$ is total amount of heat supplied and removed; $\mathrm{d}\bar{I} = \mathrm{d}\left(\bar{m}\bar{C}_p\bar{T}\right)$ change in enthalpy; $V = \bar{m}/\bar{\rho}$ volume of combustion chamber; $\bar{m}$, $\bar{\rho}$ mass and density of gas.

In eq. 1, we can distinguish the supply and removal of heat, transform it taking into account the mixing of flows with different temperatures (Khrulev et al. 2024), and write it in the following form:

$$\bar{m}\frac{\mathrm{d}\bar{q}}{\mathrm{d}\bar{t}} - \frac{U}{F}\frac{\bar{m}}{\bar{\rho}}\bar{q}_w = \bar{m}\frac{\mathrm{d}\left(\bar{C}_p\bar{T}\right)}{\mathrm{d}\bar{t}} + \bar{C}_p\bar{T}\sum_{i=1}^{n}\frac{\mathrm{d}\bar{m}_i}{\mathrm{d}\bar{t}} - \sum_{i=1}^{n}\bar{C}_{pi}\bar{T}_i\frac{\mathrm{d}\bar{m}_i}{\mathrm{d}\bar{t}} - \frac{\bar{m}}{\bar{\rho}}\frac{\partial\bar{p}}{\partial\bar{t}}, \tag{2}$$

where U, F are perimeter and cross-sectional area of the channel; $\bar{C}_{pi}\bar{T}_i$ is stagnation enthalpy of the i th flow flowing into or out of the volume V with mass flow rate $\mathrm{d}\bar{m}_i/\mathrm{d}\bar{t}$; $\mathrm{d}\bar{q}/\mathrm{d}\bar{t}$ is heat supply rate; $\bar{q}_w$ is specific heat flux into the wall; n is the number of cross sections through which air/combustion products flow into/out of the combustion chamber.

Since the length L is taken as the characteristic size of the engine, we take the cross-sectional area of the exhaust pipe F_a as the characteristic area

$$F = F_a$$

Then eq. 2 can be written in dimensionless form as follows (in the first approximation we assume that the heat exchange

surface is a pipe of constant cross-section)

$$(3)\quad \left(C_pT\sum_{i=1}^{n}\frac{dm_i}{dt}-\sum_{i=1}^{n}C_{pi}T_i\frac{dm_i}{dt}\right)\frac{F_aL}{V}+\rho\frac{dq}{dt}-\frac{UL}{F}q_w=\rho\frac{d\left(C_pT\right)}{dt}-\frac{\bar{R}_0}{\bar{C}_{p0}}\frac{dp}{dt},$$

The value of $\frac{\bar{R}_0}{\bar{C}_{p0}}$ can be written in terms of gas parameters

$$\frac{\bar{R}_0}{\bar{C}_{p0}}=\frac{\bar{R}_0}{\bar{C}_{p0}}\frac{R}{\bar{R}}\frac{\bar{C}_p}{C_p}=\frac{C_p}{R}\frac{\gamma-1}{\gamma},$$

where γ is the gas heat capacity ratio.

Thus, finally

$$(4)\quad \left(C_pT\sum_{i=1}^{n}\frac{dm_i}{dt}-\sum_{i=1}^{n}C_{pi}T_i\frac{dm_i}{dt}\right)\frac{F_aL}{V}+\rho\frac{dq}{dt}-\frac{UL}{F}q_w=\rho\frac{d\left(C_pT\right)}{dt}-\frac{\gamma-1}{\gamma}\frac{C_p}{R}\frac{dp}{dt}$$

Let us now consider the equation of state of an ideal gas:

$$\bar{p}=\frac{\bar{m}}{V}\bar{R}\bar{T}$$

Differentiating this equation with respect to time, we obtain

$$\frac{d\bar{p}}{d\bar{t}}=\frac{\bar{R}\bar{T}}{V}\sum_{i=1}^{n}\frac{d\bar{m}_i}{d\bar{t}}+\frac{\bar{m}\bar{R}}{V}\frac{d\bar{T}}{d\bar{t}}-\frac{\bar{m}\bar{R}\bar{T}}{V^2}\frac{dV}{d\bar{t}},$$

or in dimensionless form

$$\frac{dp}{dt}=F_aL\frac{RT}{V}\sum_{i=1}^{n}\frac{dm_i}{dt}+\rho R\frac{dT}{dt}-\frac{p}{V}\frac{dV}{dt}.$$

Whence:

$$(5)\quad \frac{1}{p}\frac{dp}{dt}=\frac{F_aL}{V}\frac{1}{\rho}\sum_{i=1}^{n}\frac{dm_i}{dt}+\frac{1}{T}\frac{dT}{dt}-\frac{1}{V}\frac{dV}{dt},$$

where dV/dt is the rate of change of volume (within the considered model it is equal to 0).

Now, having the basic equations, we can proceed to compiling equations describing the working process in the combustion chamber of a pulse jet engine. To do this, we will divide the pulse jet engine cycle into several sections, depending on the pressure difference between the combustion chamber and the environment, the direction of gas flow in the exhaust pipe, and the presence or absence of combustion of the fuel–air mixture.

Let us consider the pulsejet workflow from the moment of ignition of the mixture in the combustion chamber with the initial values of pressure, temperature, and velocity: $p = 1$, $T = 1$, $v = 0$. When heat is supplied to a combustion chamber with a volume of V, in general, the pressure and temperature increase, and the combustion products flow into the exhaust pipe. However, at the initial pressure in the chamber below the total pressure at the engine inlet, i.e., at $p < \pi\ (M)$, wheregas dynamic function of pressure is $\pi\ (M) = \left[1+0,5\left(\gamma-1\right)M^2\right]^{\frac{\gamma}{\gamma-1}}$, M is the flight Mach number, there is a positive pressure drop between the inlet device and the combustion chamber, the inlet valves are open, and air flows into the combustion chamber at a flow rate of dm_e/dt. Then, from eqs. 4 and 5, we obtain (approximately assuming that $d(C_pT) = C_pdT$, i.e., the heat capacity remains constant in a certain temperature range)

$$(6)\quad \begin{cases}\left[C_{p0}T_0\tau\ (M)\frac{dm_e}{dt}+C_pT\frac{dm_c}{dt}-C_pT\frac{dm_e}{dt}-C_pT\frac{dm_c}{dt}\right]\frac{F_aL}{V}+\rho\frac{dq}{dt}-\frac{UL}{F}q_w==\rho C_p\frac{dT}{dt}-\frac{\gamma-1}{\gamma}\frac{C_p}{R}\frac{dp}{dt},\\ \frac{1}{p}\frac{dp}{dt}=\frac{F_aL}{V}\frac{1}{\rho}\left(\frac{dm_e}{dt}+\frac{dm_c}{dt}\right)+\frac{1}{T}\frac{dT}{dt},\end{cases}$$

where $\tau\ (M) = 1 + 0,5\ (\gamma - 1)\ M^2$ is gas dynamic function of temperature.

Whence:

$$(7)\quad \begin{cases}\left[\frac{\tau\ (M)}{C_p}-T\right]\frac{dm_e}{dt}\frac{F_aL}{V}+\frac{\rho}{C_p}\frac{dq}{dt}-\frac{UL}{F}\frac{q_w}{C_p}=\rho\frac{dT}{dt}-\frac{\gamma-1}{\gamma R}\frac{dp}{dt},\\ \frac{dp}{dt}=\frac{F_aL}{V}RT\left(\frac{dm_e}{dt}+\frac{dm_c}{dt}\right)+\frac{p}{T}\frac{dT}{dt},\end{cases}$$

where dm_c/dt is gas flow from the combustion chamber through the nozzle.

Solving these equations for the derivatives dT/dt and dp/dt, we obtain the following system of first-order differential equations, resolved with respect to the derivative:

$$(8)\quad \begin{cases}\frac{dT}{dt}=\frac{\gamma}{C_p}\frac{dq}{dt}+(\gamma-1)\frac{F_aL}{V}\frac{dm_c}{dt}+\frac{F_aL}{V}\frac{RT}{p}\frac{dm_e}{dt}\left[\gamma\frac{\tau\ (M)}{C_p}-T\right]-\gamma\frac{RT}{C_pp}\frac{UL}{F}q_w\\ \frac{dp}{dt}=\frac{\gamma}{C_p}\frac{p}{T}\frac{dq}{dt}+\gamma RT\frac{F_aL}{V}\frac{dm_c}{dt}+\gamma\frac{\tau\ (M)}{C_p}\frac{F_aL}{V}\frac{dm_e}{dt}-\gamma\frac{R}{C_p}\frac{UL}{F}q_w\end{cases}$$

Let us now consider the individual quantities included in these equations. The dimensionless value $(F_a L)/V$, obtained as a result of reducing the equations to a dimensionless form, can be called the "complex pulsejet parameter," since, according to the system of eq. 8, the change in gas parameters in the combustion chamber depends on it. Let us denote it by the letter Λ:

$$\Lambda = \frac{F_a L}{V}$$

The value of the heat supply rate can be found using the method from Schetinkov (1965). According to this method, which is used, among other things, in the mathematical description of the non-stationary combustion mode in liquid rocket engines, the instantaneous rate of heat supply at time t is taken to be proportional to the instantaneous mass flow rate of the combustible mixture at time $t - \tau$, where τ is the ignition delay time, depending on the pressure and temperature of the gas, i.e.,

$$\frac{\mathrm{d}\bar{q}}{\mathrm{d}\bar{t}}_{t} \frac{\mathrm{d}\bar{m}_e}{\mathrm{d}\bar{t}}_{t-\tau}$$

On the other hand, the condition of balance of the energy released during combustion must be met

$$\bar{m} \int_0^{\Delta t_H} \frac{\mathrm{d}\bar{q}}{\mathrm{d}\bar{t}} \mathrm{d}\bar{t} = \bar{H}_u \eta \bar{m}_f, \tag{9}$$

where Δt_H is the time of filling the combustion chamber with the mixture; $\bar{m}$ is the mass of gas in the chamber; $\bar{m}_f$ is the mass of fuel injected into the chamber during the time Δt_H; η is the completeness of combustion.

Therefore:

$$\frac{\mathrm{d}\bar{q}}{\mathrm{d}\bar{t}} = \frac{\bar{H}_u \eta}{\bar{m}} \frac{\mathrm{d}\bar{m}_f}{\mathrm{d}\bar{t}}_{t-\tau} = \frac{\bar{H}_u \eta}{\lambda_c L_0 \bar{m}} \frac{\mathrm{d}\bar{m}_e}{\mathrm{d}\bar{t}}_{t-\tau},$$

where λ_c is air–fuel ratio; L_0 is the stoichiometric coefficient.

In dimensionless form, it will be

$$\frac{\mathrm{d}q}{\mathrm{d}t} = \Lambda \frac{H_u \eta}{\lambda_c L_0 \rho} \frac{\mathrm{d}m_e}{\mathrm{d}t}_{t-\tau} = \Lambda \frac{RT}{p} \frac{H_u \eta}{\lambda_c L_0} \frac{\mathrm{d}m_e}{\mathrm{d}t}_{t-\tau} \tag{10}$$

Equation 10 corresponds to the case when, during the starting process, the combustion chamber is gradually filled with a fuel–air mixture due to the starting boost at the engine inlet or the vacuum in the chamber. When the pressure increases $p \geq \pi$ (M), the eq. 10 should be written as

$$\frac{\mathrm{d}q}{\mathrm{d}t} = \Lambda \frac{H_u \eta}{\lambda_c L_0 \rho_M} \frac{\mathrm{d}m_e}{\mathrm{d}t}_{t-\tau},$$

where ρ_M is the gas density corresponding to the moment in time when $p = \pi$ (M).

If, during startup, it is assumed that a mixture already prepared in some way is ignited in the combustion chamber, and there is no boost at the inlet, then, obviously,

$$\rho_M = \rho_0 = 1$$

The method of calculating the rate of heat release depending on the mixture flow rate taking into account the ignition delay time, allows us to take into account the dependence of the ignition delay time on pressure and temperature, e.g., in

Fig. 3. Qualitative dependence of air flow during intake and heat release rate on time.

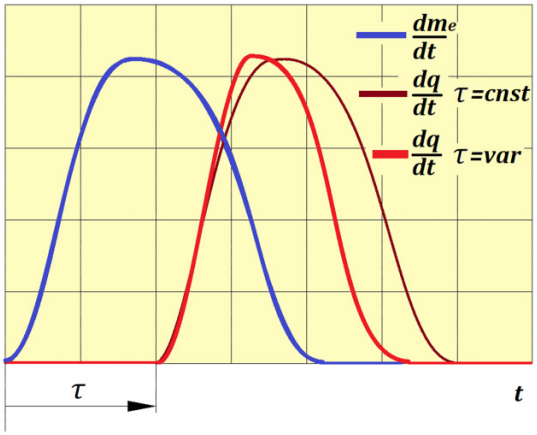

the form of the Arrhenius law for the rate of chemical reactions (Glassman and Yetter 2008):

$$\bar{\tau} = \bar{\tau}_0 \frac{\exp\left[a\left(\bar{T} - \bar{T}_0\right)\right]}{\bar{p}^b}$$

At $\bar{\tau} = \text{const}$ the heat release curve repeats the curve of the instantaneous air flow rate entering the chamber at the inlet (Fig. 3). If $\bar{\tau}$ changes during the combustion process, which corresponds to the real nature of this process, then heat release will occur over a period of time shorter than the time it takes to fill the combustion chamber.

Although such a representation of the heat release process is qualitatively close to the real one, it cannot be calculated quantitatively with high accuracy within the framework of a volumetric model. Accordingly, some basic values for the ignition delay were adopted in the model with subsequent correction for temperature and pressure using a formula corresponding to known data on fuel combustion (Schetinkov 1965) in the form

$$\tau = 0,01 m \frac{L}{a_0 p} \theta^{1,16(1-1/T)}, \tag{11}$$

where θ is a coefficient showing the effect of temperature on the ignition delay time, i.e., how many times the delay time at the current temperature decreases from time at the ambient temperature (preliminary, $\theta = 0.10$ was adopted in the model); m is the fraction of the cycle occupied by the ignition delay at the ambient temperature ($m = 0.30$ was adopted as a first approximation).

The described calculation method is not suitable for the starting cycle, since it is impossible to calculate the air flow rate without a special starting cycle model. Based on this, the process of mixture combustion and heat release during startup can be calculated approximately by another way. For this purpose, the heat release rate in the first cycle is approximated by a sinusoid, which is zero at the beginning and at the end of the combustion process, and has a maximum in the middle, and condition (9) is also satisfied

$$\frac{\mathrm{d}\bar{q}}{\mathrm{d}\bar{t}} = \frac{\bar{H}_u \eta \bar{m}_T}{\bar{m}_0 \Delta \bar{t}_c} \left\{1 + \sin\left[\frac{\pi}{2}\left(4\frac{\bar{t}}{\Delta \bar{t}_c} - 1\right)\right]\right\},$$

where $\Delta\bar{t}_c$ is the combustion time; $\bar{m}_T$ is the mass of fuel in the combustion chamber.

The value of the combustion efficiency η, according to Schetinkov (1965), strongly depends on the air–fuel ratio. This dependence was previously expressed by an approximate representation of the experimental curve $\eta = f(\lambda)$, constructed based on the data of experiments on ignition of the fuel–air mixture in a calorimetric bomb

$$\eta = \eta_0 \left[1 - 1,73\,(2-\lambda)\,(\lambda - 1,12)^2\right], \tag{12}$$

where η_0 is the maximum value of the combustion efficiency coefficient at $\lambda = 1.1$.

It is quite possible that in a pulse jet engine, especially with a lean mixture, the limits of fuel regulation and ignition may be wider than the dependence (12) allows, corresponding to other conditions. However, since there are currently no reliable data for describing volumetric pulsating combustion, the dependence (12) is used in the model under consideration. Since the length of the engine is relatively large, but the residence time of the fuel in the gas–air tract is not long, in the first approximation, it is assumed that η_0 lies within the range of 0.70–0.75 (Schmidt 1957). It is also assumed that the combustion model will be further refined as the entire algorithm for modeling the engine's working process is improved.

The instantaneous mass flow rate of air through the valve system will be equal to

$$\frac{d\bar{m}_e}{d\bar{t}} = \mu_e \bar{\rho}_e \bar{v}_e F_e,$$

Or in dimensionless form

$$\frac{dm_e}{dt} = \frac{d\bar{m}_e/d\bar{t}}{\bar{\rho}_0 \bar{a}_0 F_a} = \mu_e \rho_e v_e \frac{F_e}{F_a}. \tag{13}$$

where μ_e is the flow rate coefficient of the intake system.

The instantaneous gas flow rate through the nozzle, taking into account the "–" sign, since the flow occurs from the combustion chamber, will be equal to

$$\frac{dm_c}{dt} = -\mu_c \rho_c v_c,$$

where μ_c is the flow rate coefficient through the nozzle.

Assuming approximately that under conditions $p \geq 1$ and $v \geq 0$ a complete gas expansion occurs in the nozzle, we obtain the following expression:

$$\frac{dm_c}{dt} = -\mu_c \frac{p}{RT}\left(\frac{p_a}{p}\right)^{\frac{1}{\gamma}} v_c, \tag{14}$$

where p_a is the static pressure at the nozzle exit.

It means the boundary condition used here is the equality of the pressure at the exhaust pipe section to the ambient pressure $p_a = 1$.

The last term of eq. 8 takes into account heat losses through the walls of the engine flow path. Since heat loss occurs through all engine external surfaces, the value q_w includes the heat flow into the walls of the combustion chamber (including nozzle cone) q_{wK} and exhaust pipe q_{wT}; therefore, the total heat loss can be represented as

$$\bar{Q}_w = \bar{q}_{wK} F'_K + \bar{q}_{wT} F'_T,$$

where F'_K, F'_T are the surface areas of the combustion chamber and the exhaust pipe.

The chosen "piston analogy" model for the exhaust pipe does not allow modeling the gas flow with heat exchange there; therefore, heat losses through the walls of the exhaust pipe are taken into account in the heat balance of the combustion chamber. Then it is obvious that

$$\bar{q}_w = \bar{q}_{wK} + \bar{q}_{wT} \frac{F'_T}{F'_K},$$

whence:

$$q_w = q_{wK} + q_{wT} \frac{L}{L_K} \sqrt{\frac{F_a}{F_K}},$$

where L_K, F_K are the length and cross-sectional area of the combustion chamber.

We transform the last term in the eq. 8:

$$k \frac{RT}{C_p p} \frac{UL}{F} q_w = 4k \frac{RT}{C_p p} q_w \frac{L}{D_K} = 4k \frac{RT}{C_p p} \frac{L}{D_K} \left(q_{wK} + q_{wT} \frac{L}{L_K} \sqrt{\frac{F_a}{F_K}}\right)$$
$$= 4k \frac{RT}{C_p p} \frac{L}{D_K} \left(1 + \frac{\bar{q}_{wT}}{\bar{q}_{wK}} \frac{L}{L_K} \sqrt{\frac{F_a}{F_K}}\right) q'_{wK} = 4k \frac{RT}{C_p p} \frac{L}{D_K} q_{wK} K_w,$$

where $K_w = 1 + \frac{q_{wT}}{q_{wK}} \frac{L}{L_K} \sqrt{\frac{F_a}{F_K}}$.

In existing designs of pulsejets, on average, we get $\frac{L}{L_K} \approx 5$, $\frac{F_K}{F_a} \approx 1,85$. If we also approximately assume that $q_{wT} \approx q_{wK}$, then $K_w = 3.7$. This value can be used in approximate calculations. Thus, we obtain a certain thermal parameter of the engine's working process, characterizing heat losses through the walls of the flow part, which we denote by the letter θ

$$\theta = \frac{L}{D_K} q_{wK} K_w. \tag{15}$$

In accordance with the accepted notations, eq. 8 is finally written as

$$\begin{cases} \dfrac{dT}{dt} = \dfrac{\gamma}{C_p}\dfrac{dq}{dt} + \Lambda \dfrac{RT}{p}\left\{(\gamma - 1)\,T \dfrac{dm_c}{dt} + \left[\gamma \dfrac{\tau(M)}{C_p} - T\right]\dfrac{dm_e}{dt}\right\} - 4\gamma \dfrac{RT}{C_p p}\theta \\ \dfrac{dp}{dt} = \dfrac{\gamma}{C_p}\dfrac{p}{T}\dfrac{dq}{dt} + \gamma\Lambda\left[RT\dfrac{dm_c}{dt} + \dfrac{\tau(M)}{C_p}\dfrac{dm_e}{dt}\right] - 4\gamma\dfrac{R}{C_p}\theta. \end{cases} \tag{16}$$

The gas constants—the heat capacity ratio γ, the gas constant R and, consequently, the heat capacity at constant pressure C_p—can be represented as functions of the temperature and pressure in the combustion chamber, as well as excess air coefficient. Thus, the following relations were used to calculate in the pulsejet model

the heat capacity ratio (Guha 2001; Ceviz and Kaymaz 2005)

at $\bar{T} < 700$ K:

$$\gamma = 1 + \frac{0,40}{1 + 0,40A_x}, A_x = {t_r}^2 \frac{e^{t_r}}{(e^{t_r} - 1)^2}, t_r = \frac{3055,55}{\bar{T}},$$

at $\bar{T} \geq 700$ K:

$$\gamma = \gamma_0 - \frac{0,20}{e^{t_r}}, t_r = \frac{900}{\bar{T}}.$$

To simplify the algorithm without loss of accuracy at $\bar{T} < 700$ K the gas constant was assumed to be equal to $\bar{R} = \bar{R}_0 = 287.3$ ($R = 1.0$), and at $\bar{T} \geq 700$ K it was calculated using the formula depending on the composition of the air–fuel mixture

$$\bar{R} = \bar{R}_0 \frac{1 + \frac{r_f}{\lambda_c L_0}}{1 + \frac{1}{\lambda_c L_0}},$$

where r_f is the characteristic number of the fuel (for gasoline $r_f = 1.219$; for kerosene $r_f = 1.016$; for propane $r_f = 1.317$); λ_c is air–fuel ratio; L_0 is the stoichiometric coefficient.

In addition to those indicated, the coefficients of thermal conductivity λ and dynamic viscosity μ of air (gas) are calculated using the formulas

$$\lambda = \lambda_0 \left(\frac{\bar{T}}{273}\right)^{0.82}, \mu = \mu_0 \left(\frac{\bar{T}}{273}\right)^{0.683}.$$

Equations 16 describe the working process in the combustion chamber at the initial section of the engine starting cycle in the general case in the presence of a velocity pressure or starting boost at the inlet.

Note that the third term of the eq. 16 will be equal to zero when the pressure in the combustion chamber exceeds the velocity pressure at the inlet, and the intake valves close; also, after the end of combustion of the fuel–air mixture, the first term of the eq. 16 will disappear. In this case, the equations will be valid until the moment when the pressure in the combustion chamber due to the outflow of gas into the exhaust pipe becomes less than the total pressure at the engine inlet.

The next section of the pulsejet cycle is characterized by a vacuum in the combustion chamber ($p < 1.0$) and filling the chamber with air through the valve system. The outflow of gas from the chamber into the exhaust pipe will continue due to the kinetic energy of the gas column ("liquid piston") acquired in the previous section of the cycle. Equations 4 and 5 for this section will have the form

$$(17) \quad \begin{cases} \left[C_{p0} T_0 \tau(M) \frac{dm_e}{dt} + C_p T \frac{dm_c}{dt} - C_p T \frac{dm_e}{dt} - C_p T \frac{dm_c}{dt}\right] \Lambda - \frac{UL}{F} q_w = \rho C_p \frac{dT}{dt} \\ \frac{dp}{dt} = \Lambda R T \left(\frac{dm_e}{dt} + \frac{dm_c}{dt}\right) + \frac{p}{T}\frac{dT}{dt}. \end{cases}$$

From where, after simple transformations, we obtain the following equations:

$$(18) \quad \begin{cases} \frac{dT}{dt} = \Lambda \frac{RT}{p}\left[\frac{\tau(M)}{C_p} - T\right]\frac{dm_e}{dt} - 4\frac{RT}{C_p p}\theta \\ \frac{dp}{dt} = \Lambda R \left[\frac{\tau(M)}{C_p}\frac{dm_e}{dt} - T\frac{dm_c}{dt}\right] - 4\frac{R}{C_p}\theta. \end{cases}$$

If $1 < p < \pi(M)$, then the calculation should be carried out according to eq. 16, discarding their first terms.

Equations 18 are valid in the absence of combustion of the mixture during the filling process, i.e., until the moment of the start of combustion, corresponding to the excess of the current time of the filling process over the ignition delay time. Consequently, when heat is supplied to the gas in the combustion chamber, a term with the rate of heat release will be added to eq. 18.

The gas flow rate through the nozzle in this section of the cycle can be approximately represented as

$$(19) \quad \frac{dm_c}{dt} = \begin{cases} -\mu_c \frac{p v_c}{RT}, p < 1 \\ -\mu_c \frac{p v_c}{RT}\left(\frac{p_a}{p}\right)^{\frac{1}{\gamma}}, 1 < p < \pi(M). \end{cases}$$

If the calculation is carried out for static conditions ($M = 0$) then, obviously, $\pi(M) = 1$ and, therefore

$$(20) \quad \frac{dm_c}{dt} = -\mu_c \frac{p v_c}{RT}.$$

The next section of the cycle is characterized by a change in the direction of velocity to the opposite as a result of the braking effect of the vacuum in the combustion chamber on the gas column in the exhaust resonance pipe. Therefore, eq. 4 for this section can be written as follows:

$$(21) \quad \left[C_{p0} T_0 \tau(M) \frac{dm_e}{dt} + C_p T \frac{dm_c}{dt} - C_p T \frac{dm_e}{dt} - C_p T \frac{dm_c}{dt}\right] \Lambda + \rho \frac{dq}{dt} - \frac{UL}{F} q_w = \rho C_p \frac{dT}{dt}.$$

Carrying out obvious transformations and using eq. 5, we obtain the following equations for the gas temperature and pressure in the combustion chamber:

$$(22) \quad \begin{cases} \frac{dT}{dt} = \frac{1}{C_p}\frac{dq}{dt} + \Lambda \frac{RT}{p}\left\{\left[\frac{\tau(M)}{C_p} - T\right]\frac{dm_e}{dt} + \left(\frac{C_{pT}}{C_p}T_T - T\right)\frac{dm_c}{dt}\right\} - 4\frac{RT}{C_p p}\theta \\ \frac{dp}{dt} = \frac{1}{C_p}\frac{p}{T}\frac{dq}{dt} + \Lambda R \left[\frac{\tau(M)}{C_p}\frac{dm_e}{dt} + T_T \frac{C_{pT}}{C_p}\frac{dm_c}{dt}\right] - 4\frac{R}{C_p}\theta, \end{cases}$$

where C_{pT}, T_T are the heat capacity at constant pressure and the stagnation temperature of the gas flowing into the combustion chamber from exhaust pipe.

Since the flow in the exhaust pipe is considered adiabatic in the first approximation, then, with reverse flow, the stagnation temperature of the gas does not change: $T_T = \text{const} = T_{v_a=0}$, where $T_{v_a=0}$ is the gas temperature in the combustion chamber, corresponding to the condition $v_c = 0$.

The gas flow rate through the nozzle can be found using formulas (19) with the opposite sign, taking into account that the flow rate coefficient for the reverse flow μ_c' is close to 1.0.

As a result of heat supply in the combustion chamber, the pressure and temperature of the gas increase. The pressure becomes greater than the ambient pressure, but the gas flow from the exhaust pipe into the chamber will continue for some time, since the gas column has certain inertia. For this section of the cycle, eqs. 4 and 5 are written as

$$(23)\quad \begin{cases} \left[C_{p0}T_0\tau(M)\dfrac{dm_e}{dt} + C_pT\dfrac{dm_c}{dt} - C_pT\dfrac{dm_e}{dt} - C_pT\dfrac{dm_c}{dt}\right]\Lambda + \rho\dfrac{dq}{dt} - \dfrac{UL}{F}q_w == \rho C_p\dfrac{dT}{dt} - \dfrac{\gamma-1}{\gamma}\dfrac{C_p}{R}\dfrac{dp}{dt} \\ \dfrac{dp}{dt} = \Lambda RT\left(\dfrac{dm_e}{dt} + \dfrac{dm_c}{dt}\right) + \dfrac{p}{T}\dfrac{dT}{dt}. \end{cases}$$

By carrying out the appropriate transformations and solving eq. 23 for the derivatives dT/dt and dp/dt, we arrive at the following equations:

$$(24)\quad \begin{cases} \dfrac{dT}{dt} = \dfrac{\gamma}{C_p}\dfrac{dq}{dt} + \Lambda\dfrac{RT}{p}\left\{\left[\gamma\dfrac{\tau(M)}{C_p} - T\right]\dfrac{dm_e}{dt} + \left(\gamma\dfrac{C_{pT}}{C_p}T_T - T\right)\dfrac{dm_c}{dt}\right\} - 4\gamma\dfrac{RT}{C_pp}\theta \\ \dfrac{dp}{dt} = \dfrac{\gamma}{C_p}\dfrac{p}{T}\dfrac{dq}{dt} + \Lambda\gamma R\left[\dfrac{\tau(M)}{C_p}\dfrac{dm_e}{dt} + T_T\dfrac{C_{pT}}{C_p}\dfrac{dm_c}{dt}\right] - 4\gamma\dfrac{R}{C_p}\theta. \end{cases}$$

In the equations of system eq. 24, the second term is nonzero in the pressure range $1 < p < \pi(M)$.

For $p > \pi(M)$, and also in the case when the calculation is performed for static conditions, the equations are simplified

$$(25)\quad \begin{cases} \dfrac{dT}{dt} = \dfrac{\gamma}{C_p}\dfrac{dq}{dt} + \Lambda\dfrac{RT}{p}\left(\gamma\dfrac{C_{pT}}{C_p}T_T - T\right)\dfrac{dm_c}{dt} - 4\gamma\dfrac{RT}{C_pp}\theta \\ \dfrac{dp}{dt} = \dfrac{\gamma}{C_p}\dfrac{p}{T}\dfrac{dq}{dt} + \Lambda\gamma RT_T\dfrac{C_{pT}}{C_p}\dfrac{dm_c}{dt} - 4\gamma\dfrac{R}{C_p}\theta. \end{cases}$$

After changing the direction of the gas velocity in the exhaust pipe from reverse to direct, the calculation should be carried out according to eq. 17. In this case, in the formula for determining the rate of heat release dq/dt the value of density ρ_M must correspond to the gas density at the moment of time when $v_c = 0$.

Thus, systems of differential equations are obtained that describe the change in pressure and temperature in the combustion chamber of a pulse jet engine during the entire cycle. It is easy to see that to solve these equations, it is necessary to compose equations by which it would be possible to calculate the instantaneous air flow rate when filling the combustion chamber and the instantaneous gas flow rate when flowing out of it.

Mathematical model for describing the processes of air intake into the combustion chamber through a reed valve for a valved pulse jet engine

When determining the instantaneous air flow rate, it is most appropriate, as shown in Idelchik (1966), to reduce the total hydraulic resistance at the combustion chamber inlet to a certain control section of the inlet device or to the section opened by the valve. The first option is more cumbersome and less accurate, so the second option was used in the model. In general, the operation of the valve was described by us in Kravchenko et al. (2024), but it is necessary to clarify and supplement the existing models so that they can be used in the pulse jet engine simulation program.

For this purpose, let us consider the equation of one-dimensional motion of an ideal gas (Khrulev 2023*a*), written for an inlet channel of constant cross-section (changes in cross-section are not taken into account in the first approximation)

$$(26)\quad \frac{\partial\bar{v}}{\partial\bar{t}} + \bar{v}\frac{\partial\bar{v}}{\partial\bar{x}} = \frac{-1-\delta}{\bar{\rho}}\frac{\partial\bar{p}}{\partial\bar{x}},$$

where $\bar{t}$, $\bar{x}$ are the time and coordinate along the length; $\bar{p}$, $\bar{\rho}$ are the pressure and density of the gas; δ is the fraction of the longitudinal pressure gradient spent on friction and local resistance.

Friction and hydraulic resistance can be taken into account using the total coefficient of hydraulic resistance ξ_Σ. Then the equation of motion can be represented as

$$(27)\quad \frac{\partial\bar{v}}{\partial\bar{t}} + \bar{v}\frac{\partial\bar{v}}{\partial\bar{x}} = \frac{-1}{\bar{\rho}}\frac{\partial\bar{p}}{\partial\bar{x}} - \xi\frac{\bar{v}^2}{2L},$$

where $\xi_\Sigma = \xi_T + \xi_c$, $\xi_T = \lambda_T L/D_a$ is the coefficient of friction losses in the pipe; ξ_c is the coefficient of local resistance at the point of attachment to the volume. The coefficients ξ_T and ξ_c in calculating the flow in a pipe can be found approximately using the formulas used for steady flows (the effect of pulsations on friction (Werzner et al. 2010) can also be taken into

account, but it does not give a significant difference from a quasi-steady flow).

Now, multiplying all the terms of eq. 27 by $d\bar{x}$ and approximately considering that the air in the inlet tract behaves as an incompressible medium, we arrive at the following equation:

$$\frac{d\bar{v}}{dt}d\bar{x} + \bar{v}d\bar{v} = \frac{-d\bar{p}}{\gamma_0\bar{\rho}} - \xi_\Sigma\frac{\bar{v}^2}{2l_e}d\bar{x}. \quad (28)$$

Integrating it over $\bar{x}$, the value of which will obviously vary from 0 to l_e (the length of the input channel), taking into account eq. (5), we obtain, in the first approximation, the equation in dimensionless form

$$\frac{dv_e}{dt}\left(\frac{l_e}{L}\right) + \frac{v_e^2}{2} = \frac{-\pi(M) - p_e^*}{\gamma_0 p_e^*}\tau(M) - \xi_\Sigma\frac{v_e^2}{2}, \quad (29)$$

or

$$\frac{v_e^2}{2} = \frac{-\tau(M)}{\gamma_0}\left[\frac{\pi(M)}{p_e^*} - 1\right] - \xi_\Sigma\frac{v_e^2}{2} - \frac{dv_e}{dt}\left(\frac{l_e}{L}\right). \quad (30)$$

On the other hand, if the flow in the inlet channel is taken as quasi-stationary in the first approximation, then the total pressure loss depending on the dynamic pressure (Khrulev 2023*a*)

$$\bar{p}_0\pi(M) - \bar{p}_e^* = \xi_\Sigma\bar{\rho}_e^*\frac{\bar{v}_e^2}{2}, \quad (31)$$

where $\bar{p}_e^*$, $\bar{\rho}_e^*$ are the total pressure and density.

By reducing the equation to dimensionless form, we obtain

$$p_0\pi(M) - p_e^* = \xi_\Sigma\gamma_0\frac{\rho_e^*}{\tau(M)}\frac{v_e^2}{2}. \quad (32)$$

where, taking into account that $p_0 = 1$:

$$v_e = \sqrt{2\frac{\tau(M)}{\xi_\Sigma\gamma_0}\left[\frac{p_0}{p_e^*}\pi(M) - 1\right]}. \quad (33)$$

With a relatively short input, i.e., when $l_e \ll L$, we can neglect the last term of eq. 30, and then it will become identical to eq. 33. Therefore, the condition $l_e/L \ll 1$ actually determines the accuracy of the calculation results using the proposed method (in the completed designs of valved pulse jets (Simpson 2004; Migalin et al. 2014), the value of l_e/L usually lies in the range of 0.05–0.10).

Assuming a quasi-stationary flow, the velocity in the control section of the inlet channel can be found simply from the pressure drop (Babu 2015)

$$\bar{v}_e = \sqrt{\frac{2\gamma_0}{\gamma_0 - 1}\bar{R}_0\bar{T}_0\left[1 - \left(\frac{\bar{p}}{\bar{p}_e^*}\right)^{\frac{\gamma_0-1}{\gamma_0}}\right]}, \quad (34)$$

or in dimensionless form

$$v_e = \sqrt{\frac{2}{\gamma_0 - 1}\left[1 - \left(\frac{p}{p_e^*}\right)^{\frac{\gamma_0-1}{\gamma_0}}\right]}. \quad (35)$$

where p is pressure in the combustion chamber where air flows in.

The air density in this section is determined as

$$\rho_e = \frac{p_e^*}{R_0T_0\tau(M)}\left[1 - \frac{\gamma_0 - 1}{\tau(M)}\frac{v_e^2}{2}\right]^{\frac{1}{\gamma_0-1}}, \quad (36)$$

Fig. 4. Diagram of a plate valve for determining the hydraulic resistance coefficient.

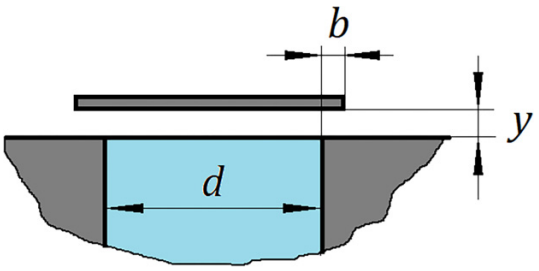

where, given that for air $R_0 = 1$, $T_0 = 1$:

$$\rho_e = \sigma\frac{\pi(M)}{\tau(M)}\left[1 - \frac{\gamma_0 - 1}{\tau(M)}\frac{v_e^2}{2}\right]^{\frac{1}{\gamma_0-1}}. \quad (37)$$

where σ is the coefficient of recovery of the total pressure in the inlet channel, which can be written as $\sigma = \bar{p}_e^*/[\bar{p}_0\pi(M)] = p_e^*/\pi(M)$.

Then the instantaneous mass flow rate of air through the valve, according to eq. 13

$$\frac{dm_e}{dt} = \mu_e\rho_e v_e\frac{F_y}{F_a}. \quad (38)$$

where $\mu_e = \frac{1}{\sqrt{1+\xi_\Sigma}}$ valve flow rate coefficient; ξ_Σ is the total coefficient of hydraulic resistance of the valve; F_y is the area opened by the valve and depends on its lift.

For a valved engine with a side entry, there is no dynamic pressure at the entry; therefore, in eqs. 34–37, the total pressure should be replaced by static pressure, and the total pressure recovery coefficient σ should be taken as 1.0.

Obviously, to determine the flow rate, it is necessary to find the hydraulic resistance of the valve. In the absence of more accurate data, you can use the known dependencies for the hydraulic resistance coefficient on the valve lift value. For example, in the first approximation, you can use the data of a plate valve, for which there is an approximate formula for the hydraulic resistance coefficient (Idelchik 1966)

$$\xi_\Sigma = 0,55 + 4\left(\frac{b}{d} - 0,1\right) + \frac{0,155}{(\bar{y}/d)^2}, \quad (39)$$

where $\bar{y}$ is valve lift; d is characteristic diameter of the opening opened by the valve; b is the value of the valve overlap of the opening when fully closed (Fig. 4).

Thus, when setting the pressure drop across the valve and the valve lift, the instantaneous air flow through the valve is determined by formula (38), taking into account (39). The question arises of how to determine the valve lift. This depends on the model chosen to describe the valve motion (Kravchenko et al. 2024).

Thus, the quasi-stationary model of the valve is obviously the simplest and assumes that the frequency of the natural oscillations of the petal is many times greater than the frequency of forced oscillations corresponding to the frequency of the engine process. In this case, the inertia of the petal movement and, first, its delay with an increase in the pressure drop can be neglected, and the problem can be considered quasi-stationary.

Fig. 5. Diagram of a petal in the form of a cantilever beam fixed at one end.

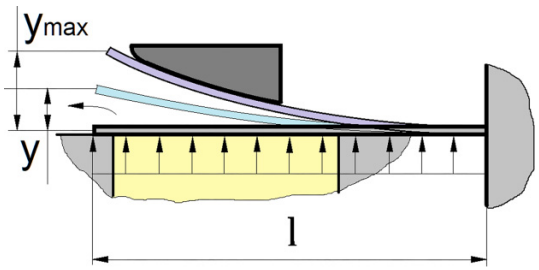

For a quasi-stationary setting, obviously, the valve deflection is completely determined by only two factors—the distributed force on the petal (pressure drop Δp) and the valve stiffness. If the valve is a beam rigidly fixed on one side, which is acted upon by a distributed force $\bar{q}$ (Fig. 5), then according to Kravchenko et al. (2024), the dependence of the petal end deflection on this force looks like this

$$\bar{y} = \frac{\bar{q} l^4}{8 \bar{E} I_x}, \tag{40}$$

where $\bar{E}$ is the elastic modulus of the petal material; I_x is the moment of inertia of the section along the axis; l is the petal length.

The petal elastic line depending on the coordinate $\bar{x}$, during petal deflection according to eq. 40, can be calculated as (Pisarenko et al. 2004)

$$\bar{y}(\bar{x}) = \frac{\bar{q}}{24 \bar{E} I_x} \left(\bar{x}^4 - 4 l \bar{x}^3 + 6 l^2 \bar{x}^2 \right). \tag{41}$$

Considering that $I_x = \delta^3 b / 12$, where δ and b are the thickness and width of the petal; $\bar{q} = \Delta \bar{p} l$, and after substituting into eq. 1 and making transformations we obtain

$$y = \frac{\bar{y}}{l} = 1,5 \frac{\Delta p}{S}, \tag{42}$$

where $\Delta p = \Delta \bar{p} / \bar{p}_0$ is the dimensionless pressure drop across the valve; $\bar{p}_0$ is the ambient pressure, and the dimensionless parameter S actually determines the petal stiffness

$$S = \frac{\bar{E}}{\bar{p}_0} \left(\frac{\delta}{l} \right)^3. \tag{43}$$

Equation 42 establishes an unambiguous dependence of the valve opening (petal deflection) on the pressure drop. However, if the natural oscillation frequency of the petal is not significantly higher than the process frequency, the quasi-stationary model may cause a significant error in calculating the air flow rate. In addition, at a high engine operating frequency (small-sized ramjet engines), there may be a delay in valve closing and a backflow of gases from the combustion chamber to the inlet channel, which cannot be taken into account using the quasi-stationary model.

As a result, the quasi-stationary valve model is applicable only at the stage of debugging the engine model, after which it must be replaced with a more realistic one. Indeed, as shown in Kravchenko et al. (2024), the real process of operation of a petal valve in a pulse jet engine is much more complex than a quasi-stationary model can provide. In fact, the model must describe a number of dynamic processes, among which, in addition to the inertial delay of the petal, it is necessary to take into account its elastic rebound from the limiter when reaching the maximum opening deviation and from the valve grid (seat) when landing on it at the moment of closing.

Fig. 6. When modeling the petal movement using a quasi-static (*a*) model, in contrast to a dynamic (*b*) model, it is impossible to take into account the delay in opening and closing of the petal, which is especially important at a high operating frequency of the engine (Kravchenko et al. 2024).

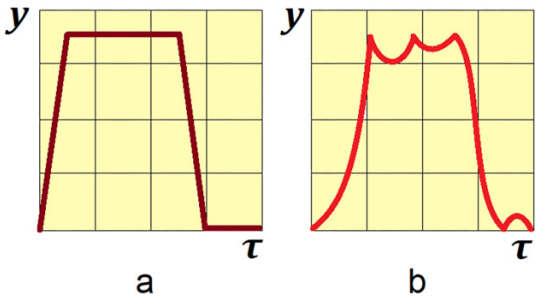

All these processes can have a significant impact on the air flow through the valve, especially when it closes late during a period of negative pressure drop, causing a backflow of air (gas, working fluid) from the combustion chamber (Kravchenko et al. 2024). Therefore, the dynamic model of the valve is a priori, a more perfect and accurate approximation to the real process than the quasi-stationary model (Fig. 6).

In the general case, the valve petal can be further considered as a beam with one side fixed (Fig. 5). The motion of such a beam can be described by a fourth-order differential equation in partial derivatives (Pisarenko et al. 2004; Kravchenko et al. 2024)

$$\frac{\partial^2}{\partial \bar{x}^2} \left(\bar{E} I_x \frac{\partial^2 \bar{y}}{\partial \bar{x}^2} \right) + m_x \frac{\partial^2 \bar{y}}{\partial \bar{t}^2} = q(\bar{x}, \bar{t}), \tag{44}$$

where m_x, $q(x, t)$ are the distributed mass of the element and the load on the beam.

Equation 44 in the general case allows one to calculate the instantaneous shape of the beam elastic line. However, in a number of works, the valve is represented in approximation as a spring-loaded concentrated mass (Fig. 7). In this case, we can use the equation of Newton's second law, which can be used to approximately determine the acceleration of the petal as the second derivative of the lift with respect to time

$$m \frac{\mathrm{d}^2 \bar{y}}{\mathrm{d} \bar{t}^2} = \Sigma \bar{F}, \tag{45}$$

where m is the concentrated mass of the petal; $\bar{F}$ is the force acting on the valve petal.

Equation 45 does not take into account viscous damping (Fig. 6*a*), which is proportional to the first derivative of the valve lift, i.e., velocity $\mathrm{d}\bar{y}/\mathrm{d}\bar{t}$ (it makes sense to take into account damping when a viscous liquid, not air, flows through the valve). In addition, in the presence of a seal, it is possible to consider not a rectilinear, but an angular motion of the

Fig. 7. Basic schemes of mechanical analogy in modeling the dynamics of petal motion: (*a*) with damper and (*b*) without a damper.

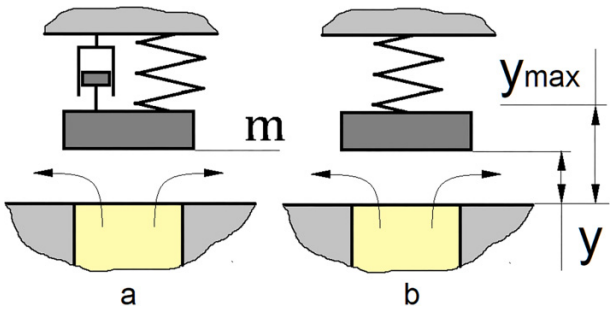

petal. However, such a representation of the problem does not provide fundamental advantages over a model of eq. 45. Therefore, when creating a model of a pulse jet engine in this work, a simpler model of a petal valve is used.

In the general case, the petal is affected by the forces of gravity, pressure, and elasticity. If we exclude the force of gravity, which is negligibly small compared to others, eq. 45 is written as

$$m\frac{\mathrm{d}^2\bar{y}}{\mathrm{d}\bar{t}^2} = -K\bar{y} + \Delta\bar{p}A, \tag{46}$$

where K is the valve stiffness; $\Delta\bar{p}$ is the pressure drop across the valve; A is the area of the petal (in the first approximation, it can be taken equal to the area of the opening opened by the petal).

The solution to eq. 46 is obtained by reducing its order by transforming it into a system of equations for the first order derivative of velocity (acceleration) and the first order derivative of lift (speed)

$$\begin{cases} \dfrac{\mathrm{d}\bar{u}}{\mathrm{d}\bar{t}} = -q\bar{y} + a\Delta\bar{p} \\ \dfrac{\mathrm{d}\bar{y}}{\mathrm{d}\bar{t}} = \bar{u} \end{cases}, \tag{47}$$

where $\bar{u}$ is the petal lift velocity; $a = bl/m$, $q = 2Sb\bar{p}_0/(3m)$.

In dimensionless form, using dimensionless variables, system eq. 47 can be written as follows:

$$\begin{cases} \theta_d\dfrac{\mathrm{d}u}{\mathrm{d}t} = \dfrac{-2}{3}Sy + \Delta p \\ \lambda\dfrac{\mathrm{d}y}{\mathrm{d}t} = u \end{cases}, \tag{48}$$

where $\theta_d = \gamma_0\rho_M\lambda\left(\frac{\delta}{l}\right)$ is the dynamic coefficient; $\rho_M = \bar{\rho}_M/\bar{\rho}_0$ is the dimensionless density of the valve petal material; $\lambda = l/L$ is the relative petal length.

It is easy to see that in the absence of acceleration (quasi-stationary model), the upper equation of system eq. 48 turns into an equation for elastic quasi-stationary opening of the valve eq. 42.

Equation 48 is solved numerically with the initial and boundary conditions (Khrulev 2023*b*; Kravchenko et al. 2024): $y = 0$, $u = 0$ at $t = 0$. The boundary conditions determine the rebound of the petal from the valve grille during landing and from the limiter at maximum opening: if $y < 0$, then $y = -\beta y$ and $u = -\beta u$ are taken, but if $y > y_{\max}$, then $y = 2y_{\max} - \beta y$ and $u = -\beta u$ are taken.

The coefficient of restitution lies in the range $\beta = 0 - 1$, which corresponds to the range from a perfectly inelastic to a perfectly elastic impact. When modeling, it is advisable to adopt the analogy of the interaction of a steel ball with a steel plate, in which the value of the coefficient β is 0,4 (Khrulev 2023*b*).

As follows from the first equation of the eq. 48, with the valve closed ($y = 0$) and a negative pressure drop (acting to close the valve), the acceleration continues to be calculated. Within the accepted boundary conditions, this may cause instability of the solution with the valve closed. To avoid this, it is advisable to impose a limitation at the smallest valve lifts, e.g., in the form: $u = 0$ at $\Delta p < 0$ and $y < 0.002$.

To calculate the air flow through the valve, it is necessary to calculate the area opened by the valve petal. For this purpose, the area of the flow section of the grate is needed, which is found from obvious geometric relationships for various valve design options. Thus, among the numerous design options, two types of valve grates can be distinguished: a flat straight line, where the valve opens a straight hole, and a wedge one. For the flow area of a flat grate with rectangular openings, the following relationship is valid

$$F_0 = \frac{1}{2}N_0L_r\left(b_1 + b_2 - 2deL\right),$$

where N_0 is the number of grate openings; L_r is the length of the petal; b_1, b_2 is the width of the petal (Fig. 8*a*); deL is the overlap of the opening by the petal.

If the petal valves are installed in a common grate and close round openings (Figs. 8*b* and 8*c*), then the dimensions are calculated as follows. First, the diameter of the opening centers D_{01}, the width of the petal b_2, the diameter D_0 and the opening area F_0 are calculated:

$$D_{01} = \frac{D_c - 2deLD + C_1}{1 + \sin\frac{\pi}{N_0}}, b_2 = D_{01}\sin\frac{\pi}{N_0} - C_1,$$
$$D_0 = b_2 - 2deL, F_0 = \frac{\pi}{4}{D_0}^2,$$

where D_c is combustion chamber diameter.

Next, the length of the petal L_{pet}, the width at the base b_1 and the area of the slots F_{dop} are calculated

$$L_{\text{pet}} = \frac{1}{2}\left(D_{01} - D_1\right) + \frac{b_2}{2}, b_1 = \frac{\pi D_1}{N_0} - C_1, F_{\text{dop}} = C_1L_{\text{pet}},$$

where D_1 is the diameter of the petal seal (Fig. 8*b*).

For a wedge grate (Fig. 9), the area opened by the valve can be calculated as follows:

$$F_0 = N_0h_r\left(b_2 - 2deL\right).$$

The height of the flow section h_r is taken as the maximum possible petal lift $y_{\max}$. If the area F_0 is greater than the area of the flow section of the inlet device F_e, then a correction $y_{\max}$ is introduced according to the formula:

$$y_{\max} = \frac{F_e}{N_0\left(b_2 - 2deL\right)}.$$

The area of the flow section opened by the petals is calculated based on the geometry of the grate. For this purpose,

Fig. 8. Design of a straight valve grate: (*a*) with rectangular openings, (*b*) with round openings, (*c*) petal shape, and (*d*) shape of slots between petals.

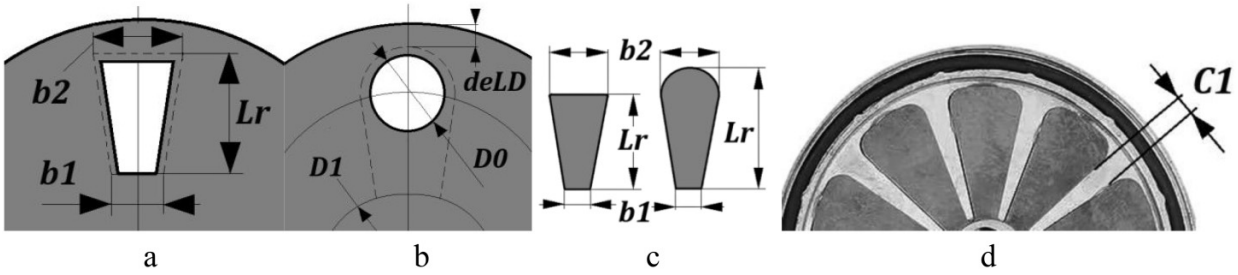

Fig. 9. Design of a wedge grate: (*a*) flow section opened by the petals and (*b*) petal shape.

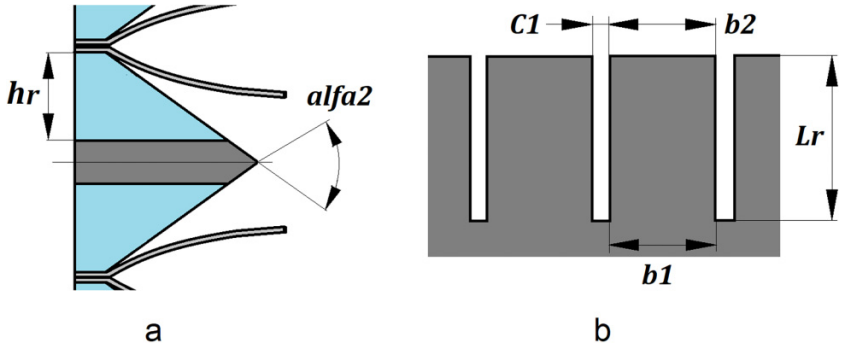

a calculation cycle is organized for sections of the petal with a length of $dx = L_{pet}/N$, where N is the number of sections. The calculation assumes that the elastic line of the petal is quasi-stationary, which allows calculating the instantaneous lift along the length using eq. 41.

The area of the lateral section opened by the petal on each section dx will be

$$f_x = 0.5\,(y_x + y_{x-dx})\,dx,$$

the current instantaneous lift angle of the petal α_x using the formula

$$\tan\alpha_x = 0.5\,(y_i - y_{i-1})\,/dx.$$

and the total lateral area of the petal is determined by numerical integration over the length of the petal

$$F = \sum_{0}^{L_{pet}} f_x.$$

Due to the slot, the area F is adjusted according to the condition: if $F > 0.5F_{dop}$ then $F = 0.5F_{dop}$.

For a straight grate with a rounded petal, the total area is approximately

$$F_y = N_0\left(\pi b_2 y + 2F + \frac{{b_2}^2}{2}\tan\alpha_L\right),$$

where $\tan\alpha_L$ corresponds to the angle at the free end of the petal.

For a wedge grate, the total area is

$$F_y = N_0\,(b_2 y + 2F)\,.$$

If the lateral area F_y exceeds the area of the grate opening F_0 it is assumed that $F_y = F_0$. Such restrictions are introduced into the model to eliminate errors and increase the stability of the solution.

Thus, all the quantities included in eq. 38 allow us to determine the instantaneous air flow through the valve system of all types under consideration.

Model of gas flow in a resonance tube of a pulse jet engine

Within the framework of the chosen "piston" analogy model ("liquid piston"), we will consider the gas movement along the exhaust pipe from the beginning of combustion of the fuel–air mixture in the combustion chamber. This process can be described as follows: due to the increase in pressure in the chamber, the air that was in the pipe during the ignition of the mixture will begin to accelerate due to its expulsion by combustion products entering the pipe from the chamber (Fig. 2). The method of approximate integration of the equation of gas motion (28) for this problem was previously performed by us in Khrulev (2023*a*), but requires some clarification.

Integration is performed from the center of the combustion chamber, where it can be approximately assumed that the gas is stationary, to the exhaust pipe exit:

$$(49)\quad \int_{-x_K}^{1}\frac{dv}{dt}dx + \int_{v_K}^{v_a} v dv = \frac{-1}{\gamma_0}\int_{p}^{p_a}\frac{dp}{\rho} - \int_{-x_K}^{1}\xi\frac{v^2}{2}dx,$$

where $x_K = \bar{x}_K/L_p$ is the relative distance from the nozzle (cone) exit to the center of the combustion chamber; $L_p = L - \bar{x}_K$ is resonance pipe length.

The second term of the equation will obviously be equal to

$$\int_{v_K}^{v_a} v\mathrm{d}v = \frac{v_a^2}{2}.$$

According to the accepted assumption about the "piston" analogy of gas motion in a pipe, the velocity at the nozzle outlet v_c and at the section of the resonant pipe v_a are equated to each other. Then the last term of the equation can be represented as

$$\int_{-x_K}^{1} \xi \frac{v^2}{2} dx = \xi_c \frac{v_c^2}{2} x_K + \xi_T \frac{v_a^2}{2} \approx \frac{v_a^2}{2} (\xi_T + x_K \xi_c), \tag{50}$$

where $\xi_T = \lambda_T L/D_a$ is the coefficient of friction losses in the pipe; ξ_c is the coefficient of local resistance of the nozzle.

Taking this into account, eq. (36) can be written as follows:

$$\int_{-x_K}^{1} \frac{\mathrm{d}v}{\mathrm{d}t} \mathrm{d}x = \frac{-1}{\gamma_0} \int_{p}^{p_a} \frac{\mathrm{d}p}{\rho} - K_\xi \frac{v_a^2}{2}, \tag{51}$$

where $K_\xi = 1 + \xi_T + x_K \xi_c$ is the coefficient taking into account friction and local resistance influence on velocity variation.

Accurate calculation of the coefficients ξ_T and ξ_c for non-stationary flow in pipes is difficult due to the lack of reliable experimental data on the effect of pulsations on hydraulic resistance. For this purpose, in this work the flow was assumed to be quasi-stationary, and approximate formulas used for stationary flows (Idelchik 1966) were used.

Let us consider the left-hand side of eq. (51). For an incompressible gas, it follows from the continuity equation that $vF = \text{const}$. Therefore, the gas velocity in any section of the pipe:

$$v = v_a \frac{F_a}{F}.$$

Whence, differentiating with respect to time, we obtain

$$\frac{\mathrm{d}v}{\mathrm{d}t} \approx \frac{\mathrm{d}v_a}{\mathrm{d}t} \frac{F_a}{F}. \tag{52}$$

In result, we get

$$\int_{-x_K}^{1} \frac{\mathrm{d}v}{\mathrm{d}t} \mathrm{d}x = \int_{-x_K}^{1} \frac{\mathrm{d}v_a}{\mathrm{d}t} \frac{F_a}{F} \mathrm{d}x = \frac{\mathrm{d}v_a}{\mathrm{d}t} \int_{-x_K}^{1} \frac{F_a}{F} \mathrm{d}x. \tag{53}$$

Let's find $\int_{-x_K}^{1} \frac{F_a}{F} \mathrm{d}x$. Obviously

$$\begin{aligned} \int_{-x_K}^{1} \frac{F_a}{F} \mathrm{d}x = \int_{-x_K}^{0} \frac{F_a}{F} \mathrm{d}x + \int_{0}^{1} \mathrm{d}x = 1 + \int_{-x_K}^{0} \frac{F_a}{F} \mathrm{d}x = 1 + \int_{-x_K}^{-x_c} \frac{F_a}{F} \mathrm{d}x \\ + \int_{-x_c}^{0} \frac{F_a}{F} \mathrm{d}x = 1 + \frac{F_a}{F_K} (x_K - x_c) + \int_{-x_c}^{0} \frac{F_a}{F} \mathrm{d}x, \end{aligned} \tag{54}$$

where x_c is the relative length of the nozzle.

Further transformations of the right-hand side of eq. 54, described by us in detail in Khrulev (2023*a*), yield the following result:

$$\int_{-x_c}^{0} \frac{F_a}{F} \mathrm{d}x \approx \frac{1}{1 - \frac{0.05}{\Lambda}}. \tag{55}$$

It is easy to see that the obtained value is, in essence, a certain correction factor to the length of the exhaust pipe, allowing one to take into account the influence of the combustion chamber length in the total length of the pipe. Since the complex parameter Λ in existing engines fluctuates in the range from 1.5 to 2.5, then failure to take into account the length of the combustion chamber will lead to an error of about 3%.

Thus, eq. 51 is written as

$$\frac{\mathrm{d}v_a}{\mathrm{d}t} \frac{1}{1 - \frac{0.05}{\Lambda}} = \frac{-1}{\gamma_0} \int_{p}^{p_a} \frac{\mathrm{d}p}{\rho} - K_\xi \frac{v_a^2}{2}, \tag{56}$$

where coefficient K_ξ can be expressed through Λ: $K_\xi \approx 1 + \xi_T + 0,25 \frac{\xi_c}{\Lambda}$.

Let us now consider the right-hand side of eq. 56. The density ρ in the denominator is the density of the gas in the exhaust pipe. Since the air that was in the pipe at the initial moment is pushed out by the combustion products, we make the assumption that there is no mixing between the combustion products and the air. Then the "air–combustion products" boundary will move along the pipe and at some point in time will move away from the nozzle exit by a distance x.

The pipe contains gases with different densities, and it is possible to find some average (reduced) density of the gas. In this case, we will also take into account the density of the gas in the combustion chamber, since eq. 56 describes the movement of gas from the center of the combustion chamber to the end of the exhaust pipe. We will write the equation for the reduced density in the form (Khrulev 2023*a*):

$$\rho_{pr} (V + F_a L) = \rho V + \rho_x F_a x + \rho_0' F_a (1 - x), \tag{57}$$

where ρ_x is the density of combustion products in the exhaust pipe; ρ_0' is the density of air in the exhaust pipe.

Let ρ_{pr} be proportional to ρ over some period of time, i.e.,: $\rho_{pr} = r\rho$, where $r = \text{const}$. Then,

$$r = \frac{\rho_{pr}}{\rho} = \frac{\Lambda}{1 + \Lambda} \left[\frac{1}{\Lambda} + x \left(\frac{\rho_x}{\rho} \right) + (1 - x) \left(\frac{\rho_0'}{\rho} \right) \right]. \tag{58}$$

We can write the gas densities included in eq. 58 as

$$\rho = \frac{p}{RT}, \rho_x = \frac{p}{RT} \left(\frac{p_a}{p} \right)^{\frac{1}{\gamma}}, \rho_0' = \frac{p_0}{R_0 T_0} \left(\frac{p}{p_0} \right)^{\frac{1}{\gamma_0}} = p^{\frac{1}{\gamma_0}}. \tag{59}$$

Therefore,

$$r = \frac{\Lambda}{1 + \Lambda} \left[\frac{1}{\Lambda} + x \left(\frac{p_a}{p} \right)^{\frac{1}{\gamma}} + (1 - x) RT \left(\frac{1}{p} \right)^{\frac{\gamma_0 - 1}{\gamma_0}} \right]. \tag{60}$$

Let us assume that the gas density in the chamber depends adiabatically on the pressure, i.e.,

$$\rho = C p^{\frac{1}{\gamma}},$$

where $C = \frac{p^{\frac{\gamma - 1}{\gamma}}}{T}$.

Then the corresponding term in eq. 56 can be represented as

$$(61)\quad \frac{-1}{\gamma_0}\int_p^{p_a}\frac{dp}{\rho}=\frac{-1}{\gamma_0}\int_p^{p_a}\frac{dp}{rCp^{\frac{1}{\gamma}}}=\frac{\gamma}{\gamma-1}\frac{RT}{\gamma_0}\frac{1}{r}\left[1-\left(\frac{p_a}{p}\right)^{\frac{\gamma-1}{\gamma}}\right].$$

By transforming eq. 56 taking into account expressions 60 and 61, we finally obtain

$$(62)\quad \frac{dv_a}{dt}=\left(1-\frac{0.05}{\Lambda}\right)\left\{\frac{\gamma}{\gamma-1}\left(1+\frac{1}{\Lambda}\right)\times\frac{RT}{\gamma_0}\frac{1-\left(\frac{p_a}{p}\right)^{\frac{\gamma-1}{\gamma}}}{\frac{1}{\Lambda}+x\left(\frac{p_a}{p}\right)^{\frac{1}{\gamma}}+(1-x)RT\left(\frac{1}{p}\right)^{\frac{\gamma_0-1}{\gamma_0}}}-K_\xi\frac{v_a^2}{2}\right\}.$$

This equation is valid for the positive direction of gas velocity in the pipe when the pressure in the combustion chamber is greater than the static pressure at the outlet of the exhaust pipe. In the next section of the cycle, with an unchanged direction of flow velocity, the pressure in the chamber will become less than the pressure at the outlet. In this case, the gas densities will be approximately equal to

$$(63)\quad \rho\approx\rho_x\approx\frac{p}{RT},\ \rho_0'=\frac{p_0}{R_0T_0}\left(\frac{p}{p_0}\right)^{\frac{1}{\gamma_0}}=\left(\frac{1}{p}\right)^{\frac{-1}{\gamma_0}}.$$

wherefrom:

$$(64)\quad r=\frac{\Lambda}{1+\Lambda}\left[\frac{1}{\Lambda}+x+(1-x)RT\left(\frac{1}{p}\right)^{\frac{\gamma_0-1}{\gamma_0}}\right].$$

Considering that in this section of the cycle the changes in the gas parameters in the combustion chamber are small due to the air flowing into the chamber, it can be assumed that the gas density is constant over a sufficiently small time interval, i.e.,

$$\rho=\frac{p}{RT}=\text{const}.$$

Then, having made the appropriate transformations of eq. 56, we obtain

$$(65)\quad \frac{dv_a}{dt}=\left(1-\frac{0.05}{\Lambda}\right)\times\left\{\left(1+\frac{1}{\Lambda}\right)\frac{RT}{\gamma_0}\frac{\frac{p_a}{p}-1}{\frac{1}{\Lambda}+x+(1-x)RT\left(\frac{1}{p}\right)^{\frac{\gamma_0-1}{\gamma_0}}}-K_\xi\frac{v_a^2}{2}\right\}.$$

When the direction of the gas velocity in the pipe changes to the opposite when integrating the equation of motion (49), the upper limits of integration should be changed to lower ones (and vice versa). Obviously, in this case the signs of the corresponding terms of eq. 56 will change. Considering that

$$(66)\quad \rho\approx\frac{p}{RT},\ \rho_x\approx\frac{p_T}{R_TT_T},\ \rho_0'\approx\frac{p_0}{R_0T_0}\left(\frac{p_a}{p_T}\right)^{\frac{\gamma_0-1}{\gamma_0}},$$

we obtain the following equation:

$$(67)\quad \frac{dv_a}{dt}=\left(1-\frac{0.05}{\Lambda}\right)\left\{\left(1+\frac{1}{\Lambda}\right)\times\frac{RT}{\gamma_0}\frac{\frac{p_a}{p}-1}{\frac{1}{\Lambda}+\frac{p_T}{p}\left[x\frac{RT}{R_TT_T}+(1-x)\frac{RT}{R_aT_a}\left(\frac{1}{p}\right)^{\frac{\gamma_0-1}{\gamma_0}}\right]}-K_\xi\frac{v_a^2}{2}\right\}.$$

When the pressure in the combustion chamber increases above the static pressure at the exhaust pipe section, we obtain expressions for the gas density similar to the previous case. Considering that the gas density in the chamber can also be approximately written as

$$\rho\approx\frac{p}{RT},$$

we arrive at eq. 67. In the next section of the cycle, when the direction of the gas velocity changes to positive, eq. 62 will be valid too. The air density in the pipe when the direction of velocity changes from reverse to direct can be approximately written as follows:

$$(68)\quad \rho_0'\approx\frac{p'}{R_aT_a}\left(\frac{p_a}{p'}\right)^{\frac{\gamma_0-1}{\gamma_0}}\left(\frac{p}{p'}\right)^{\frac{1}{\gamma_0}}=\frac{p_a^{\frac{\gamma_0-1}{\gamma_0}}}{R_aT_a}p^{\frac{1}{\gamma_0}},$$

where p' is the pressure in the chamber corresponding to $v_a=0$.

Consequently, in eqs. 62 and 65 the denominator should be multiplied by the value $p_a^{\frac{\gamma_0-1}{\gamma_0}}/(R_aT_a)$, i.e., for $p\geq p_a$:

$$(69)\quad \frac{dv_a}{dt}=\left(1-\frac{0.05}{\Lambda}\right)\left[\frac{\gamma}{\gamma-1}\left(1+\frac{1}{\Lambda}\right)\times\frac{RT}{\gamma_0}\frac{1-\left(\frac{p_a}{p}\right)^{\frac{\gamma-1}{\gamma}}}{\frac{1}{\Lambda}+x\left(\frac{p_a}{p}\right)^{\frac{1}{\gamma}}+(1-x)\frac{RT}{R_aT_a}\left(\frac{p_a}{p}\right)^{\frac{\gamma_0-1}{\gamma_0}}}-K_\xi\frac{v_a^2}{2}\right].$$

For $p<p_a$

$$(70)\quad \frac{dv_a}{dt}=\left(1-\frac{0.05}{\Lambda}\right)\left[\left(1+\frac{1}{\Lambda}\right)\times\frac{RT}{k_0}\frac{\frac{p_a}{p}-1}{\frac{1}{\Lambda}+x+(1-x)\frac{RT}{R_aT_a}\left(\frac{p_a}{p}\right)^{\frac{\gamma_0-1}{\gamma_0}}}-K_\xi\frac{v_a^2}{2}\right].$$

It should be noted that if the calculation is performed for static conditions ($M=0$, $H=0$), then the static parameters at the exhaust pipe section can be equated to the environmental parameters ($p_a=1$, $T_a=1$, $R_a=1$), and eqs. 67, 69, and 70 are somewhat simplified.

Equations 67, 69, and 70 allow us to calculate the gas velocity at the nozzle exit. If the gas in the pipe moves as an incompressible medium, then the velocity at the pipe inlet is equal to the velocity at the outlet, i.e., $v_a=v_c$. If we approximately assume that the pressure in the pipe is constant

during flow in the exhaust pipe, then we can use a simple relationship for the boundary coordinate and its velocity

$$x = 1 + \int_{t_0}^{t} v_a \mathrm{d}t. \quad (71)$$

If during the outflow the value of x, found by numerical integration of eq. 71, becomes greater than or equal to 1, then this means that the air is completely pushed out of the exhaust pipe. Further, during subsequent outflow at some point in time the velocity v_a will change sign, which will mean the beginning of air suction from the environment into the exhaust pipe.

Thus, the equations found allow us to approximately calculate the dynamics of gas movement along the engine exhaust pipe and determine the gas velocity at the nozzle and exhaust pipe section. On the one hand, together with eqs. 16–25, they constitute a complete system of equations for the working process of a valve-type pulsating air-breathing engine, and on the other hand, makes it possible to find the main parameters of the engine, by which we can judge the efficiency of its working process and the influence of various factors on it.

Model of gas and air flow in the intake canal of a valveless pulsejet engine

In a valveless pulse jet engine, obviously, there is no valve system (Fig. 2*b*), but there is an intake pipe that performs a dual task: supplying air to the combustion chamber when there is a vacuum in it and releasing gases from the chamber when the pressure increases, creating thrust.

The main problem in describing the process of air or gas flow through the intake pipe is related to the fact that, unlike a valved engine, in a valveless engine, when a vacuum occurs in the combustion chamber, air begins to flow with a significant delay. That is, at first the flow in the intake pipe reverses, but for some time residual hot gases that are in the pipe still enter the chamber. And only after cold air enters the pipe and fills the entire pipe, the combustion chamber begins to fill (Fig. 10).

Thus, the assumptions for describing this process remain the same as for the resonant pipe. That is, in addition to the movement of gases and air within the framework of the "liquid piston" analogy, it is necessary to assume the absence of mixing of cold air with gases. For this purpose, let's consider the equation of motion (28), written for a pipe of length l_e and a part of the combustion chamber from the beginning of the pipe to the point $-y_c$, where the gas velocity can be conditionally assumed to be 0

$$\frac{\mathrm{d}v}{\mathrm{d}t}\mathrm{d}y + v\mathrm{d}v = \frac{-\mathrm{d}p}{\gamma_0 \rho} - \xi_\Sigma \frac{v^2}{2}\mathrm{d}y. \quad (72)$$

where y is the relative (to the pipe length l_e) coordinate of the air-gas boundary, measured from the inlet pipe cutoff.

Let's integrate the equation from the point determined by the coordinate $-y_c$ to the pipe cutoff:

$$\int_{-y_c}^{l_e} \frac{\mathrm{d}v}{\mathrm{d}t}\mathrm{d}y + \int_{0}^{v_e} v\mathrm{d}v = \frac{-1}{\gamma_0}\int_{p}^{p_a} \frac{\mathrm{d}p}{\rho} - \int_{-y_c}^{l_e} \xi_\Sigma \frac{v^2}{2}\mathrm{d}y. \quad (73)$$

Fig. 10. The flow diagram of air and gas in the intake pipe within the framework of the "piston" analogy ("liquid piston"), adopted in the model: (*a*) the beginning of air flow into the pipe; (*b*) the beginning of the process of air intake into the combustion chamber; (*c*) the beginning of air expulsion from the pipe; and (*d*) gas outflow from the combustion chamber through the pipe.

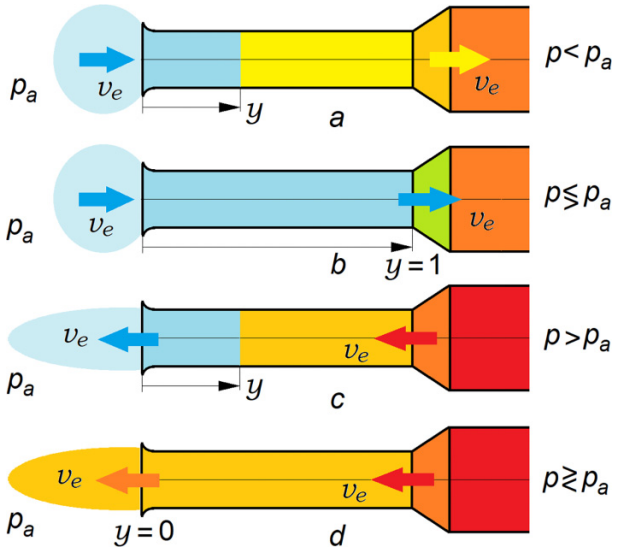

Obviously,

$$\int_{0}^{v_e} v\mathrm{d}v = \frac{{v_e}^2}{2}. \quad (74)$$

In addition,

$$\int_{-y_c}^{l_e} \xi_\Sigma \frac{v^2}{2}\mathrm{d}y = \frac{{v_e}^2}{2}\int_{-y_c}^{l_e} \xi_\Sigma \mathrm{d}y = \frac{{v_e}^2}{2}(1+\delta)\left(\xi_c \delta + \xi_f\right), \quad (75)$$

where $\delta = y_c/l_e$; ξ_c is the coefficient of hydraulic resistance of the narrowing section from the chamber to the pipe; $\xi_f = \lambda_T l_e/D_e$ is the friction coefficient.

Considering that $y_c \ll l_e$, we can simplify eq. 75

$$\int_{-y_c}^{l_e} \xi_\Sigma \frac{v^2}{2}\mathrm{d}y = \frac{{v_e}^2}{2}\left(\xi_c \delta + \xi_f\right). \quad (76)$$

Let us now consider the density of gas and air in the pipe. By analogy with the resonance pipe (57), the average (reduced) density of gas in the absence of mixing of hot gas with density ρ' and cold air with density ρ'_0 can be approximately written as

$$\rho_{pr} = \rho'_0(1-y) + \rho' y. \quad (77)$$

That is, at $y \leq 0$ the air is completely pushed out of the pipe, at $0 < y < 1$ the air enters the pipe, and at $y \geq 1$ the air completely fills the pipe, which means the process of air intake into the combustion chamber.

If we apply a similar technique 58–63 to the intake pipe, as was done for the resonance pipe, we get:

$$r = \frac{\rho_{pr}}{\rho} = \frac{\rho'_0(1-y) + \rho' y}{\rho}. \quad (78)$$

Then for a positive pressure drop between the chamber and the pipe outlet ($p \geq p_a$):

$$(79)\quad \frac{1}{\gamma_0}\int_p^{p_a}\frac{\mathrm{d}p}{\rho} = \int_p^{p_a}\frac{\mathrm{d}p}{Cp^{\frac{1}{\gamma}}} = \frac{\gamma}{\gamma-1}\frac{RT}{\gamma_0}\frac{1}{r}\left[1-\left(\frac{p_a}{p}\right)^{\frac{\gamma-1}{\gamma}}\right] = \frac{\gamma}{\gamma-1}\frac{RT}{\gamma_0}\frac{\left[1-\left(\frac{p_a}{p}\right)^{\frac{\gamma-1}{\gamma}}\right]}{\rho_0'(1-y)+\rho' y}.$$

When the pressure in the chamber decreases below the pressure at the pipe outlet, i.e., when $p < p_a$ the pressure ratio should be reversed by p/p_a. The densities included in eq. 79 can be represented as follows (the inlet pipe of a valveless engine is always located against the flight direction, so there is no dynamic pressure at the inlet):

$$(80)\quad \rho' = \frac{p}{RT}\left(\frac{p_a}{p}\right)^{\frac{1}{\gamma}},\ \rho' = \frac{p_a}{R_0 T_a}\left(\frac{p}{p_a}\right)^{\frac{1}{\gamma_0}}.$$

Integrating the acceleration along the length of the pipe yields

$$(81)\quad \int_{-y_c}^{l_e}\frac{\mathrm{d}v}{\mathrm{d}t}\mathrm{d}y = \frac{\mathrm{d}v_e}{\mathrm{d}t}\int_{-y_c}^{l_e}\frac{F_e}{F}\mathrm{d}y = \frac{\mathrm{d}v_e}{\mathrm{d}t}\left(\frac{l_e}{L}\right)\left(1+\frac{y_c}{l_e}\frac{D_e}{D_c}\right) = \frac{\mathrm{d}v_e}{\mathrm{d}t}\left(\frac{l_e}{L}\right)(1+\varepsilon),$$

where $\varepsilon = \frac{y_c}{l_e}\frac{D_e}{D_c} = \delta\frac{D_e}{D_c}$ is a value 1.5–2 times smaller than δ, and therefore also much smaller than unity.

Substituting expressions 74, 76, 80, and 81 into 73, we obtain

$$(82)\quad \frac{\mathrm{d}v_e}{\mathrm{d}t} = \frac{L}{l_e}\frac{\gamma}{\gamma-1}\frac{RT}{\gamma_0}\frac{1-\left(\frac{p_a}{p}\right)^{\frac{\gamma-1}{\gamma}}}{\rho_0'(1-y)+\rho' y} - K_{\xi e}\frac{L}{l_e}\frac{{v_e}^2}{2},$$

where the coefficient $K_{\xi e} = 1 + \xi_c\delta + \xi_f$.

Equation 82, therefore, determines not only the velocity in the pipe, but also the movement (displacement) of the air–gas boundary along the pipe with velocity v_e, the coordinate of which is determined by numerical integration:

$$(83)\quad y = 1 + \int_0^t v_e \mathrm{d}t.$$

Equation 83 is solved numerically together with eq. 82. The moment of the beginning of air intake (and it is taken in the model as the end of the previous and the beginning of the new cycle) will be the moment in time at which cold air reaches the combustion chamber, i.e., when y becomes equal to 1.

Accounting for heat exchange with the environment

Obviously, within the framework of the considered model, only an approximate accounting of thermal processes is possible. For internal heat exchange, it is assumed that the process of heat exchange with the walls is concentrated in the combustion chamber, but the calculation is carried out for the process of gas flow in a resonance tube. Then, for the convective q_{wc} and radiant q_{wr} heat flux into the wall, the formula is valid (Rohsenow et al. 1998):

$$(84)\quad \bar{q}_{wK} = \bar{q}_{wc} + \bar{q}_{wr} = \bar{\alpha}_{wi}\left(\bar{T} - \bar{T}_w\right) + \varepsilon\sigma\left(\bar{T}^4 - \bar{T}_w{}^4\right),$$

where $\bar{T}_w$ is the wall temperature; $\alpha_{wi} = Nu\lambda/D_a$ is the heat transfer coefficient; ε is the wall emissivity; $\sigma = 5.64\cdot10^{-8}$ W/m^{2}K^4 is the Stefan–Boltzmann constant.

Model (Arpaci et al. 1993) allows taking into account the pulsating nature of the flow and the influence of the frequency f_c and the amplitude v_0 of the velocity pulsation on heat transfer using the velocity coefficient K_a:

$$Nu = Nu_m K_a,\ K_a = \left[1 + 0,21\frac{\bar{v}_0}{\bar{v}_{am}}\left(1 + 7,36\frac{\bar{f}_c - 46}{\bar{v}_{am}}D_a\right)\right]^{0,75},$$

where $Nu_m = 0.0243Re^{0,75}$ is the quasi-stationary Nusselt number calculated from the average gas velocity v_{am}; $Re = \bar{v}_{am}D_a/\nu$ is the Reynolds number; $\nu = \mu/\rho$ is the kinematic viscosity coefficient of the gas.

The value of the heat flux from the gas to the wall q_{wK} according to eq. 15 is included in the differential equations for the temperature and pressure in the combustion chamber. From the outside, the equation for the total heat flux looks similar (we neglect the thermal conductivity of the thin wall and the difference between the temperatures inside and outside):

$$(85)\quad \bar{q}_{we} = \bar{q}_{wc} + \bar{q}_{wr} = \bar{\alpha}_{we}\left(\bar{T}_w - \bar{T}_0\right) + \varepsilon\sigma\left(\bar{T}_w{}^4 - \bar{T}_0{}^4\right),$$

where the convective part $Nu = 0.036Re^{0.8}Pr^{0.33}$ is calculated depending on the flight speed v_0 (Lienhard and Lienhard 2008).

Since all thermal processes depend on the wall temperature, which is included in eqs. 84 and 85, it is important to calculate it. This can be done using the heat balance equation (Khrulev and Saraev 2021), written for a wall with thickness δ_w:

$$(86)\quad \frac{\mathrm{d}T_w}{\mathrm{d}t} = \frac{q_{wK} - q_{we}}{C_w\rho_w\delta_w}.$$

According to eq. 86, the wall heating rate is proportional to the heat flux and inversely proportional to the mass and heat capacity of the wall. It is characteristic that this equation has the same entry in dimensional and dimensionless form. In the latter case, it includes the relative (to the length of the resonance tube) wall thickness.

Equation 86 is solved numerically and calculates the temperature to the state of thermal equilibrium. However, a feature of the wall temperature calculation in this model is its short time (only 7–12 engine cycles), during which the wall does not have time to quickly respond to changes in parameters, including flight speed. To bring the wall temperature closer to the desired state of thermal equilibrium, the approximate initial value of the wall temperature is first calculated using the formula:

$$(87)\quad \bar{T}_w = 650\left(1 + 1.167e^{-1.64M_0}\right).$$

This formula is obtained by approximate approximation of the calculation data for blowing air over a heated pipe (Lienhard and Lienhard 2008). Then the wall temperature is actually specified depending on the engine operating mode and external conditions.

Calculation of the main engine parameters

The solution of differential eqs. 16, 18, 21, 24, and 25 for the temperature and pressure in the combustion chamber together with eq. 48 for the valve lobe in a valve engine, eqs. 62, 65, and 67–71 for the gas velocity in the resonance tube, as well as eqs. 82 and 83 for the gas velocity in the intake pipe (for a valveless engine) is performed by the numerical integration method. In this work, the second order Runge-Kutta method was used (Biringen and Chow 2011) with the initial conditions: at $t = 0$ $p = 1$, $T = 1$, $v_a = v_c = v_x = v_y = 0$, $x = y = 0$. The use of higher order integration methods is impractical, since it does not have a noticeable effect on the accuracy of calculations, but significantly complicates the algorithm and reduces the speed of calculations.

The result of integration is the dependence of instantaneous parameters on the current cycle time

$$p, T, v_a, v_e, x, y, \frac{dm_e}{dt}, \frac{dm_c}{dt} = f(t). \quad (88)$$

Simultaneously with the integration of the specified equations, integration is carried out and the values for the cycle of the main parameters of the simulated engine are determined. Thus, the second air flow through the engine can be represented as

$$\bar{M}_e = \bar{m}_e \bar{f}, \quad (89)$$

where $\bar{m}_e$ is the mass of air entering the engine during the cycle; $\bar{f}$ is the frequency of cycles (the number of cycles per second).

The mass of air $\bar{m}_e$ is determined by numerical summation over the time step

$$\bar{m}_e = \int_{\bar{t}_H}^{\bar{t}_K} \left(\frac{d\bar{m}_e}{d\bar{t}}\right) d\bar{t} = \mu_e \int_{\bar{t}_H}^{\bar{t}_K} \bar{\rho}_e \bar{v}_e F_y d\bar{t}, \quad (90)$$

where $\bar{t}_H$, $\bar{t}_K$ are the timemoments of the beginning and the end of the filling process.

Using dimensionless variables, one can also find the mass of air received during the cycle in dimensionless form:

$$m_e = \frac{\bar{m}_e}{\bar{p}_0 V / (\bar{R}_0 \bar{T}_0)} = \Lambda \Phi \int_{t_H}^{t_K} \frac{F_y}{F_a} m_e v_e dt. \quad (91)$$

The dimensionless cycle frequency is determined after calculating the cycle by the formula

$$f = \frac{1}{t_c} = \bar{f} \frac{L}{a_0}, \quad (92)$$

where t_c is dimensionless cycle time, counted from the moment air begins to enter the combustion chamber.

Then, substituting relations 96 and 97 into formula 95, we obtain the air flow rate

$$\bar{M}_e = \frac{m_e f}{\Lambda} \sqrt{\frac{\gamma_0}{\bar{R}_0 \bar{T}_0}} \bar{p}_0 F_a. \quad (93)$$

The value $\frac{m_e f}{\Lambda}$ represents the dimensionless air flow through the engine

$$M_e = \frac{m_e f}{\Lambda} = \frac{\bar{M}_e}{\bar{\rho}_0 \bar{a}_0 F_a}. \quad (94)$$

Accordingly, fuel consumption can be represented as

$$\bar{M}_f = \frac{\bar{M}_e}{\lambda_c L_0}, M_f = \frac{m_e f}{\lambda L_0 \Lambda}. \quad (95)$$

The instantaneous thrust of the engine will be equal to

$$\bar{F}_t = \bar{v}_a \frac{d\bar{m}_a}{d\bar{t}} - \bar{V}_n \frac{d\bar{m}_e}{d\bar{t}}, \quad (96)$$

from where the average thrust over time is obtained by the same numerical summation over the time step:

$$\bar{F}_{en} = \bar{f} \int_{\bar{t}_a}^{\bar{t}_b} \bar{v}_a \left(\frac{d\bar{m}_a}{d\bar{t}}\right) d\bar{t} - \bar{f} \int_{\bar{t}_H}^{\bar{t}_K} \bar{V}_n \left(\frac{d\bar{m}_e}{d\bar{t}}\right) d\bar{t}, \quad (97)$$

where $\bar{t}_a$, $\bar{t}_b$ are the time moments limiting the period of flow from the pipe ($v_a > 0$).

The parameters in dimensionless form are calculated to obtain generalized dependencies by the similarity criterias Λ, Φ, S, θ. Since $\frac{d\bar{m}_a}{d\bar{t}} = \bar{\rho}_a \bar{v}_a F_a$, then in dimensionless form the thrust can be expressed by the following relationship:

$$F_{en} = \frac{\bar{F}_d}{\gamma_0 \bar{p}_a F_a} = f \int_{t_a}^{t_b} \rho_a v_a^2 dt - f \Phi \Lambda \int_{t_H}^{t_K} \rho_e v_e dt. \quad (98)$$

For the gas density included in eq. 98, it should be taken into account that air and residual gases are alternately expelled from the exhaust pipe. Therefore, taking into account expressions 66 for $v_a > 0$, it is accepted:

$$\rho_a =$$

The specific fuel consumption is determined by the formula

$$\overline{\mathrm{TSFC}} = 3600 \frac{\bar{M}_f}{\bar{F}_{en}}, \quad (100)$$

and the specific engine thrust

$$\bar{F}_S = \frac{\bar{F}_{en}}{\bar{M}_e} = \frac{3600}{\overline{\mathrm{TSFC}} \lambda_c L_0}. \quad (101)$$

In addition to the thrust determined in accordance with formula 97, the so-called “clean” (net) thrust can also be calculated (Rolls-Royce 1996). Due to the high wall temperature in known aircraft designs, the pulsating engine is placed outside. In this case, an additional aerodynamic drag force X, appears in flight, which is determined by the flight speed and the aerodynamic drag coefficient C_x of the engine placed in the oncoming flow. Then the net thrust can be written as

$$\bar{F}_n = \bar{F}_d - \bar{X} = \bar{F}_d - C_x \bar{\rho}_0 \frac{\bar{V}_n^2}{2},$$

where coefficient C_x is determined from known test data of various bodies and elements of aircraft (Hoerner 1992) (preliminary it was assumed that $C_x = 0.045$ for direct entry, $C_x = 0.05$ for an aerodynamic fairing with a side entry, $C_x = 0.2$ for a valveless toroidal engine).

Development and debugging of a pulse jet engine simulation program

As part of the implementation of the project to create a working model of a pulse jet engine for a wide range of users,

Fig. 11. Title page of the Pulsejet-Sim program.

Table 1. Architecture of the Pulsejet-Sim program.

Layer	Technology	Purpose	Advantages
Backend	Django 4.2 LTS, Django REST Framework, distributed Celery task queue, in-memoryKV-storageRedis	Logical separation pattern MVC (Model-View-Controller), ORM (object-relational mapping), asynchronous REST API computations	LTS (long-term support), security
Database	DBMS—Database Management System PostgreSQL 15	ACID transactions (atomicity, consistency, isolation, durability), GiST indexes (generalized search tree)	Scalability, maturity
Frontend	jQuery 3.7, Bootstrap 5.3, AJAX/JSON (Asynchronous JavaScript And XML/JavaScript Object Notation)	Adaptive layout RWD (Responsive Web Design)	Small JS footprint (volume of scripts)
DevOps	Containerization Docker Compose, Gunicorn, Nginx, CI/CD (Continuous Integration/Continuous Delivery)	Containerization, autodeployment	Repeatability, horizontal scalability

Table 2. Platform of the algorithmic model.

No.	Module	Function	Key techniques
1	Data-entry and metadata service	Input validation, unit normalization, auto	Bootstrap validation, Pydantic (schema validation)
2	Preset manager	Saving profiles, versioning and sharing via UUID	PostgreSQL, JSONB (binary JSON), OpenAPI v3
3	Compute engine	Asynchronous calculations, caching, export CSV (Comma	Celery 5.5 + Redis

the Pulsejet-Sim program (Fig. 11) was developed as an online service for calculating and optimizing the parameters of a pulse jet engine (Pulsejet-Sim 2025).

The platform is built as a single-page application with an open architecture of REST API (Representational State Transfer Application Programming Interface) web services. Data structure (stack) and database management systems are the following: Python 3, Django 4.2 LTS, PostgreSQL 15, jQuery 3.7, Bootstrap 5.3.

The program deployment process takes place in the GNU/Linux + Gunicorn + Nginx environment. The step-by-step graphical user interface (GUI) dynamically suggests acceptable ranges and prevents input errors.

When developing software, it is necessary to take into account that pulse jet engines are characterized by their design simplicity, but have a high T/W-ratio (thrust-to-weight ratio), are sensitive to the accuracy of geometry and are critical to acoustic resonance effects. This is confirmed by numerical studies using the method CDF (computional fluid dynamics) (Isac et al. 2014; Tegné 2022). Pulsejet-Sim makes these calculations available through a browser, reducing the barrier to entry for research and development engineers and UAV designers. The web service architecture is presented in Table 1.

The algorithmic model platform consists of three logical modules (Table 2), which exchange data via REST API in JSON and MsgPack (MessagePack is a binary serialization format).

S3-compatible storage (Simple Storage Service) holds the results; worker nodes are automatically scaled from 1 to 192 vCPU (virtual CPU).

During data entry (data-entry and metadata service), each form field is instantly validated on the client with HTML attributes pattern, min, max. After the onBlur event (fo-

Fig. 12. General pulse jet engine data entry field.

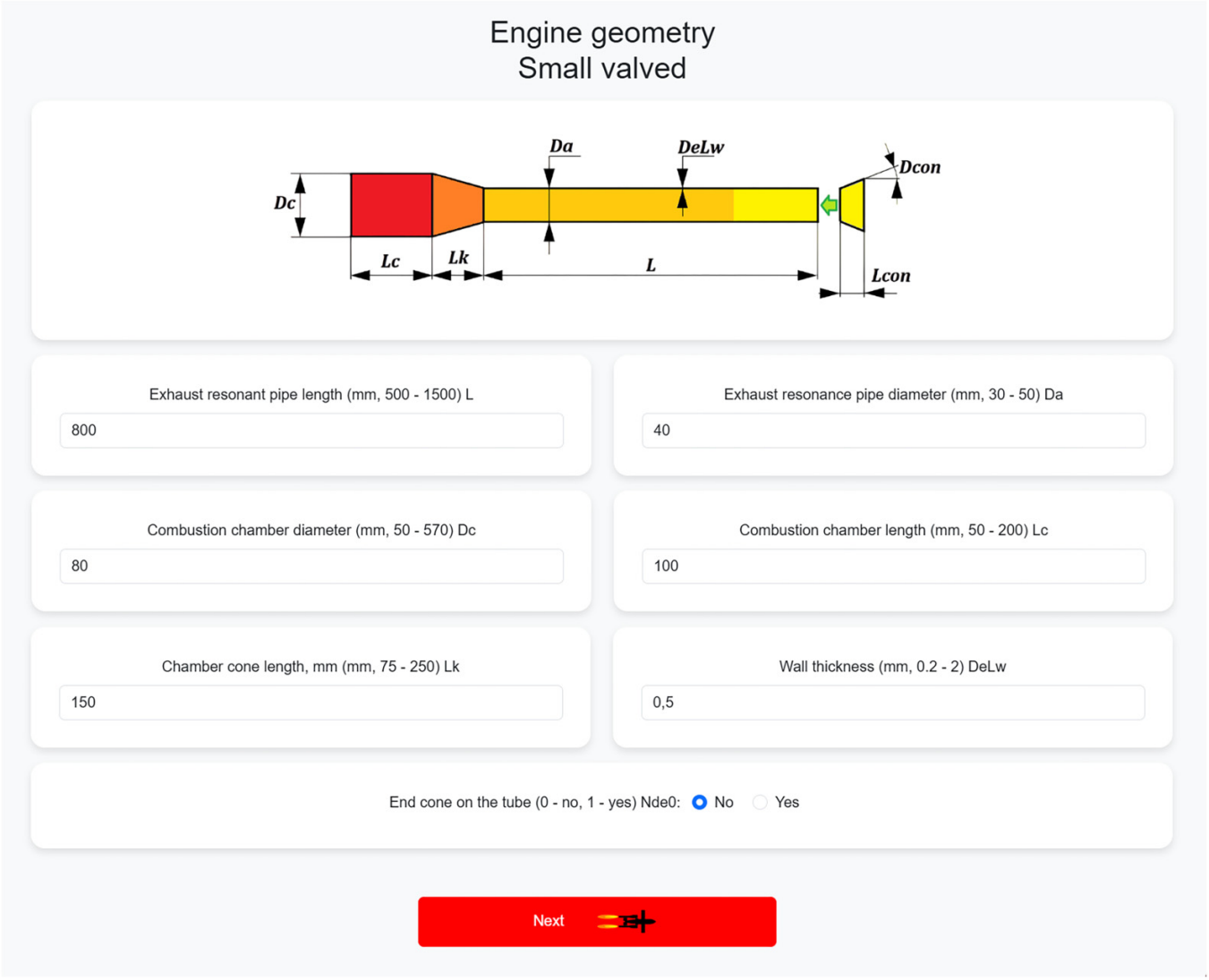

cus loss event), the client part of the Front-end application sends a PATCH request (HTTP PATCH—partial resource update) to/api/meta/, where the server part of the Back-end made in the form of:

class InletSchema (BaseModel):
diameter: conf.confloat(gt = 0.015, lt = 0.30)
length: conf.confloat(gt = 0.10, lt = 2.00),
and then normalizes the data to an adimensional form and returns a MetaPayload object, which dynamically updates the UI (user interface).

The general appearance of a part of the input field for the initial data are shown in Figs. 12 and 13.

The preset manager includes the following functions:

1. Factory presets—12 basic configurations are available at first launch (Argus As 014, Solar PJ32, etc.).
2. User-defined sets—each set of parameters is serialized as JSON Schema Draft-2020–12 (JavaScript Object Notation Schema—data structure description format) and stored in presets. This allows data to be integrated into external PLM/CAD software (Product Lifecycle Management/Computer-Aided Design) via simple HTTP GET (HTTP GET—resource retrieval method).
3. Snapshot export—any preset or calculation result is exported to the following formats:
   - CSV (comma-separated values—tabular data);
   - JSON Schema (object description for API—Application Programming);
   - PNG (portable network graphics—raster graphic format).

The compute engine works as follows. When you click "Calculate," a task object is generated. Then, the distributed Celery task queue distributes these tasks between worker nodes (execution nodes) with an autoscale of 1–192 vCPU (virtual CPU—virtual processor core).

Each worker loads the cache of thermodynamic tables in pickle format (≈12 MB; Python-serialization of objects) into

Fig. 13. Input field for the intake system of a valveless engine.

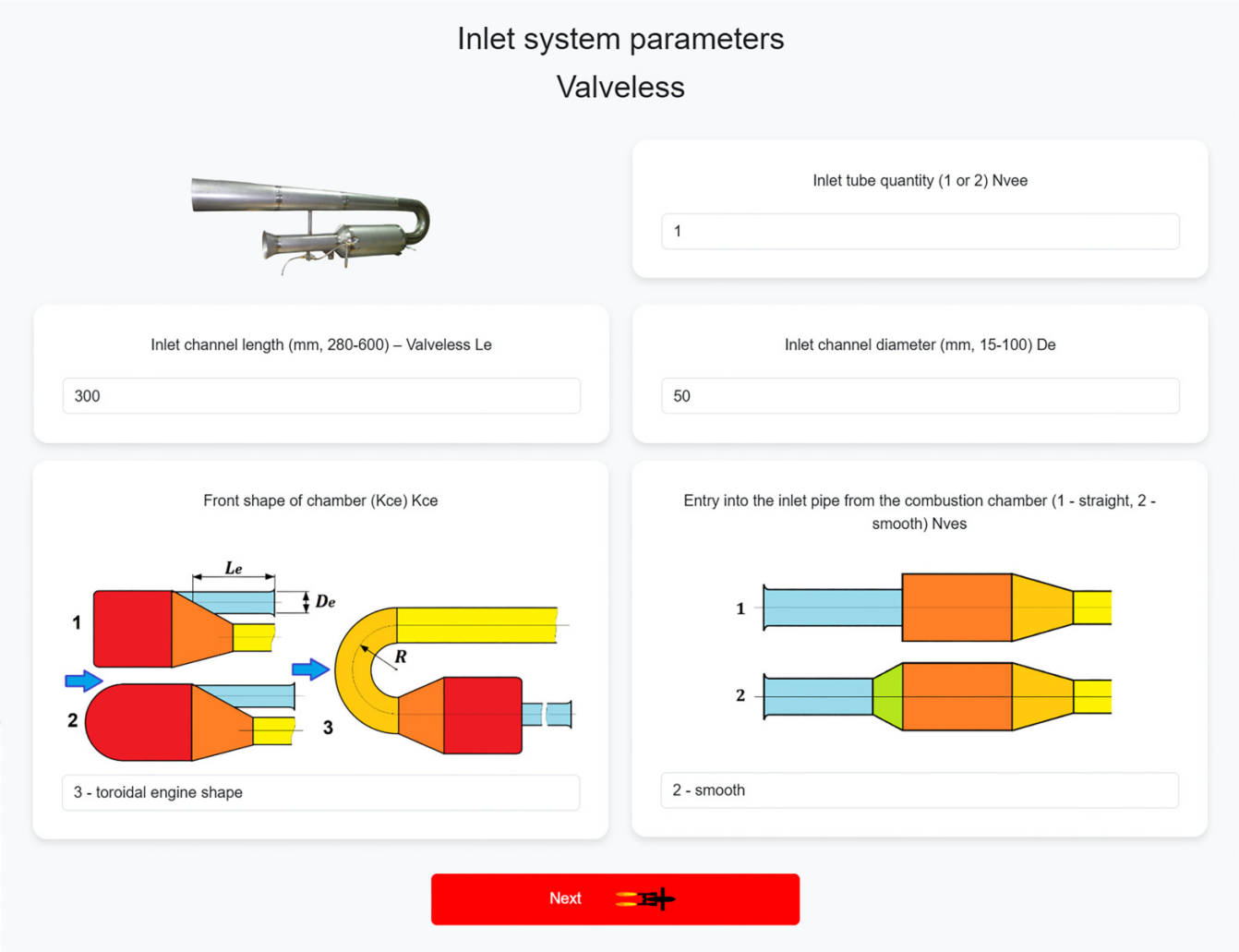

shared memory, which reduces the cold start to ≈ 120 ms. The calculation process is accompanied by graphical construction of diagrams of the calculated parameters (Figs. 14 and 15).

Once completed, the results are stored in the results table (Fig. 16) and in S3-compatible storage (Amazon Simple Storage), from where they can be downloaded by the client or received by a third-party system via a webhook (HTTP callback).

The program implements reuse scenarios. CI-loop of the design department (Wikipedia 2025*a*): Jenkins (Jenkins 2025) calls/api/run/with a JSON set of parameters, waits for callback/api/webhook/, loads an STL file (3D printing format). The process can be described as follows: demo presets are imported, one variable is changed, and the export and comparison of results are performed in MATLAB via a REST client (REST—Representational State Transfer, an architectural style of web services).

Thus, the three-level modular organization Data-Entry → Preset Manager → Compute Engine provides:

- fast prototyping (hot-reload schema—instant reloading of schemas);
- data reliability (strict validation + versioning—strict validation and version control);
- horizontal scaling of calculations without changes in the business logic code.

The user interface design has the following features:

1. Wizard UX (Wizard User Experience—step-by-step input) reduces cognitive load.
2. DOM-binding (Document Object Model) via jQuery.on("change") instantly shows recommendations.
3. NUI/CLI synergy (Natural User Interface—natural interface of gestures/clicks/Command-Line Interface—command line) allows you to run the model both from the browser and from the terminal.
4. ARIA components (Accessible Rich Internet Applications) provide accessibility.

In addition, important properties of the system are adaptability and reactivity, provided by the following means:

Fig. 14. Graphical representation of a pulse jet engine start-up process and entering the operating mode.

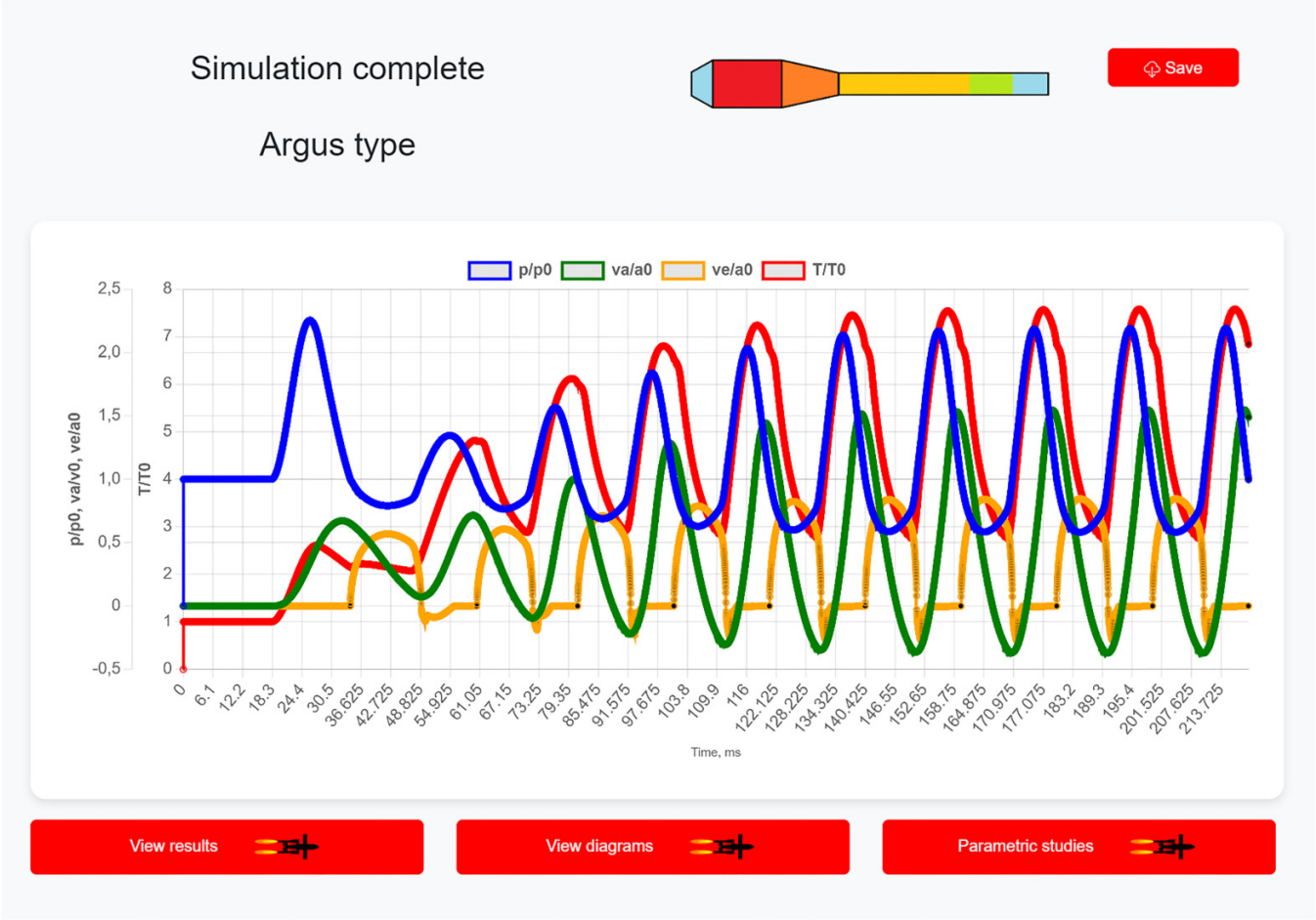

Fig. 15. View of parameter diagrams in a cycle that can be viewed and saved by the user.

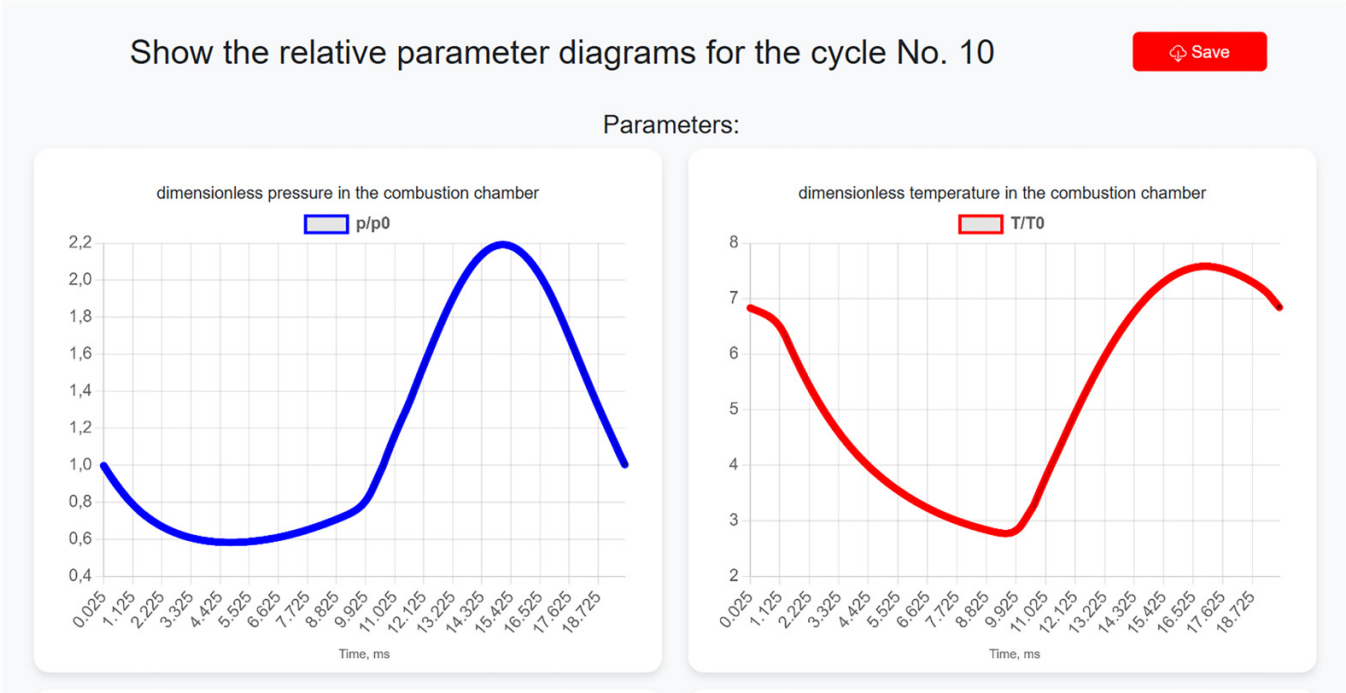

Fig. 16. Output of calculation results of the main engine parameters.

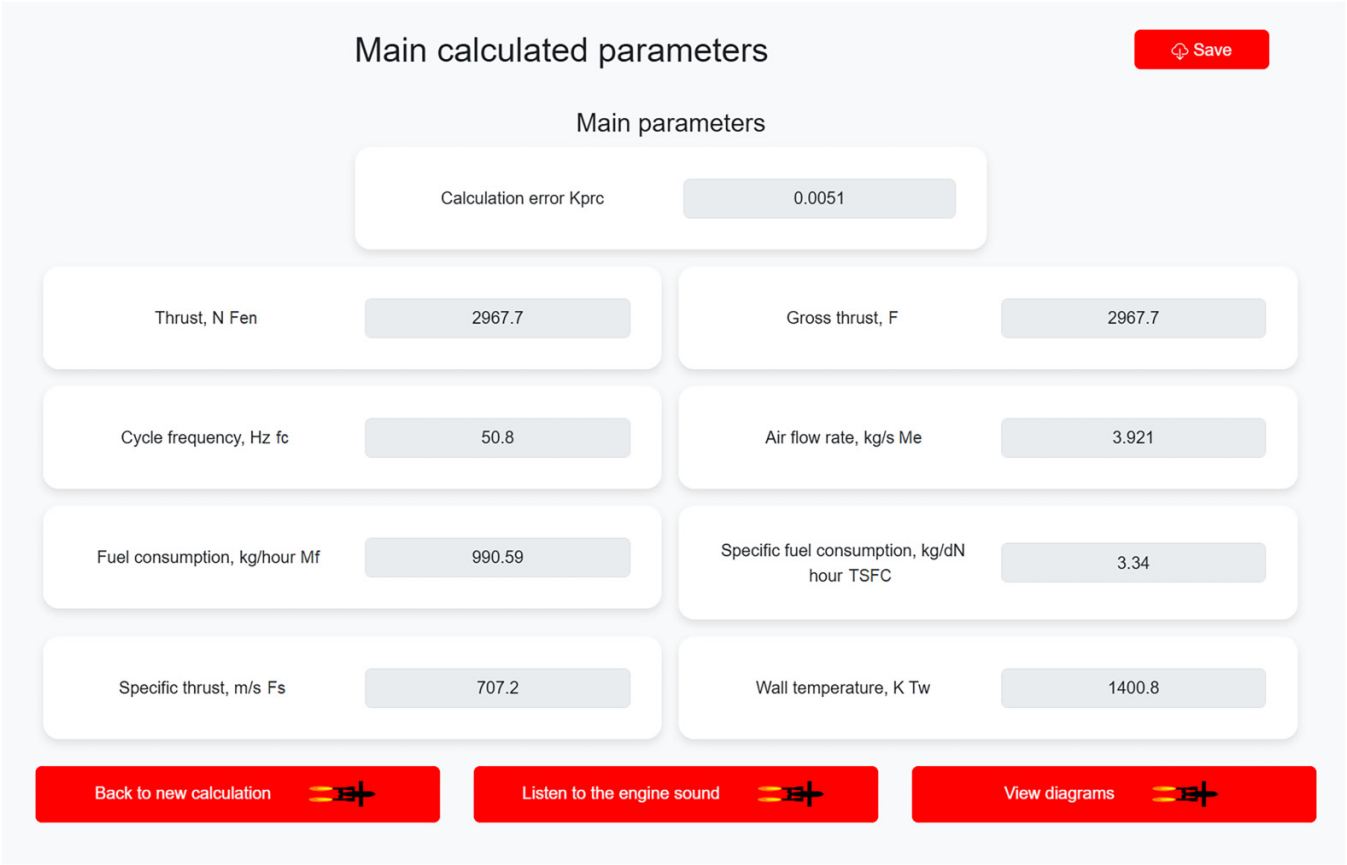

Table 3. Main advantages of Pulsejet-Sim program.

Category	Pulsejet-Sim advantages	Explanation
CAPEX → OPEX (Capital Expenditure/Operational Expenditure)	Zero-Install, Pay-per-Run	Reduced TCO (Total Cost of Ownership)
Elasticity	Scale 1–10 000 vCPUs per second	On-demand cluster
Licensing	Usage-based billing	No hard core licenses
DR (disaster recovery)	Geo-redundant, RAID-6	Automatic backups
Security	TLS 1.3, separate VPCs (Virtual Private Cloud), SOC 2/ISO 27001 certifications	Regular patches without downtime
PUE (power usage effectiveness)	≤1.15 in the cloud	Energy savings up to 40%
Continuous delivery (CD)—continuous delivery/deployment of software; a practice in which code changes undergo automated tests and can be deployed to production at any time.	CI/CD → Docker → K8s (Kubernetes)	Instant updates

- Dynamic DOM binding—dynamic DOM binding. jQuery events <code> .on("change") </code> (jQuery 2025) call the REST endpoint (architectural style of web services)/api/suggest/, which returns a new array of suggested values.
- Responsive grid—adaptive Bootstrap grid <code> col-lg-4 col-md-6</code> (Bootstrap 2025) provides an optimal HDPI (High Dots Per Inch—high ppi) view—from mobile devices to 4 K monitors (3840 × 2160 px).

The approach used in the program has its advantages. Thus, when using NUI/CLI synergy—a combination of NUI and CLI, step-by-step input reduces cognitive load (cognitive load theory) (Clark and Kimmons 2023) and reduces the average session time by 34% compared to the "all-in-one" form. Data integrity is also ensured. Validation on the client (JS—JavaScript), server (Django forms) and in the model (pydantic schema—Python data validation library) (Pydantic 2025) minimizes GIGO risks (Garbage In, Garbage Out).

As a result, unlike classic CAE systems (computer-aided engineering) in the form of desktop engineering and simulation software packages that require a local HPC (high-performance computing) cluster with increased performance, lengthy installation and expensive static "seat/core"

Fig. 17. General view of parametric calculation results in Pulsejet-Sim (example with invalid point excluded).

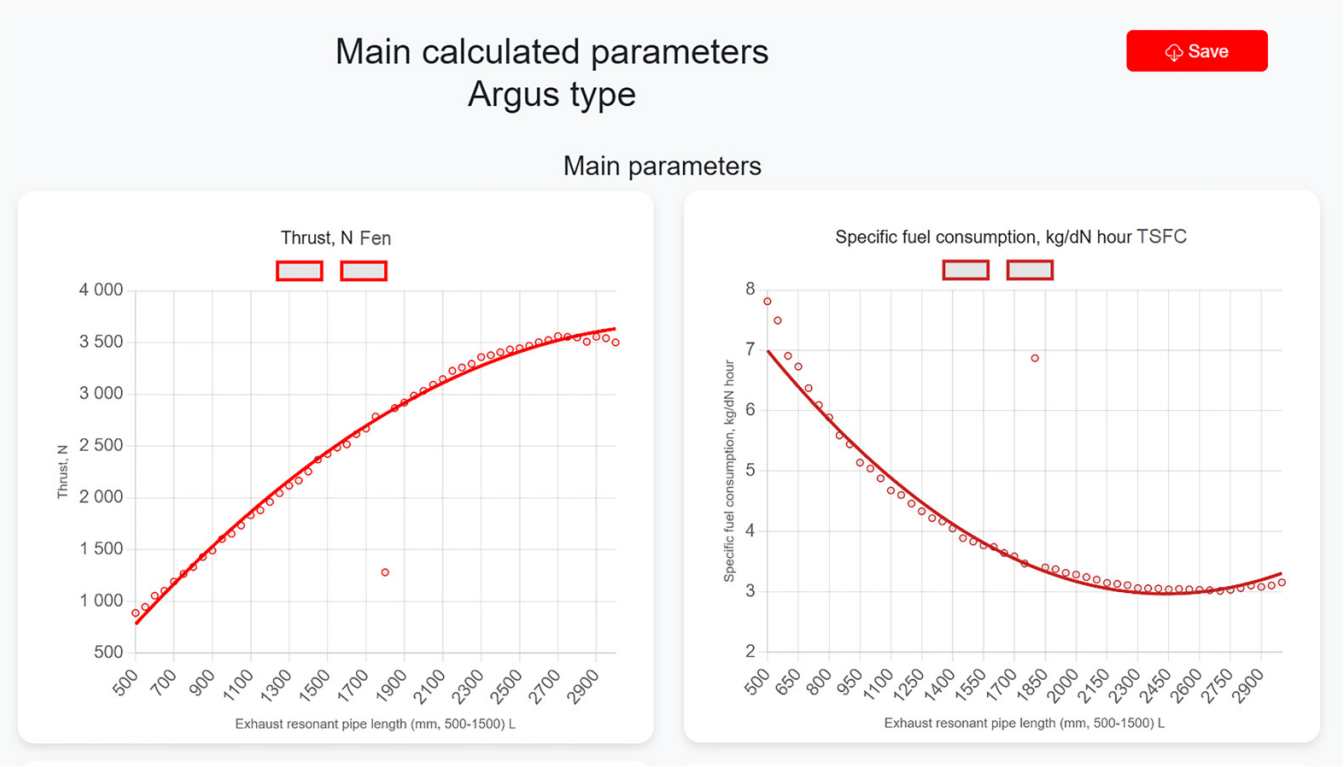

Fig. 18. Results of modeling using the Pulsejet-Sim program of changes in instantaneous parameters of gas and air, as well as the lift of the valve petal in the pulsejet working cycle for valved Solar PJ32 pulse jet engine (Litke et al. 2005).

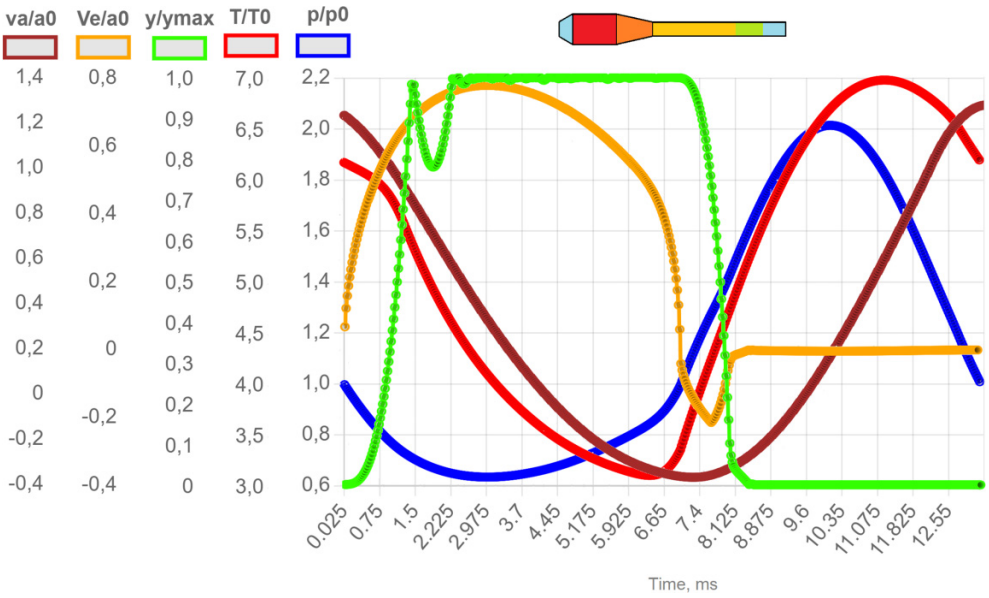

licenses. Pulsejet-1.0 implements a cloud-based SaaS (Software as a Service) model. This ensures work directly in the browser, payment for launch and instant scaling without the need to own hardware. The main advantages of the developed program are presented in Table 3.

As a result, the measured average duration of the Pulsejet-Sim thermogasdynamic run is 1.8 s on an AMD EPYC 9454 node (192 vCPU—virtual CPU, virtual processor core) with caching of thermodynamic tables—the performance equivalent to a local cluster with 128 physical cores, but without the cost of the macquisition and maintenance.For research groups, this means more DSE (design-space exploration) iterations with the same budget ceiling, and for startups—the ability to run engineering sim-

Fig. 19. Results of modeling of changes in instantaneous parameters of gas and air, as well as the air–gas boundary in the intake pipe in the pulsejet working cycle for the test valveless pulse jet engine.

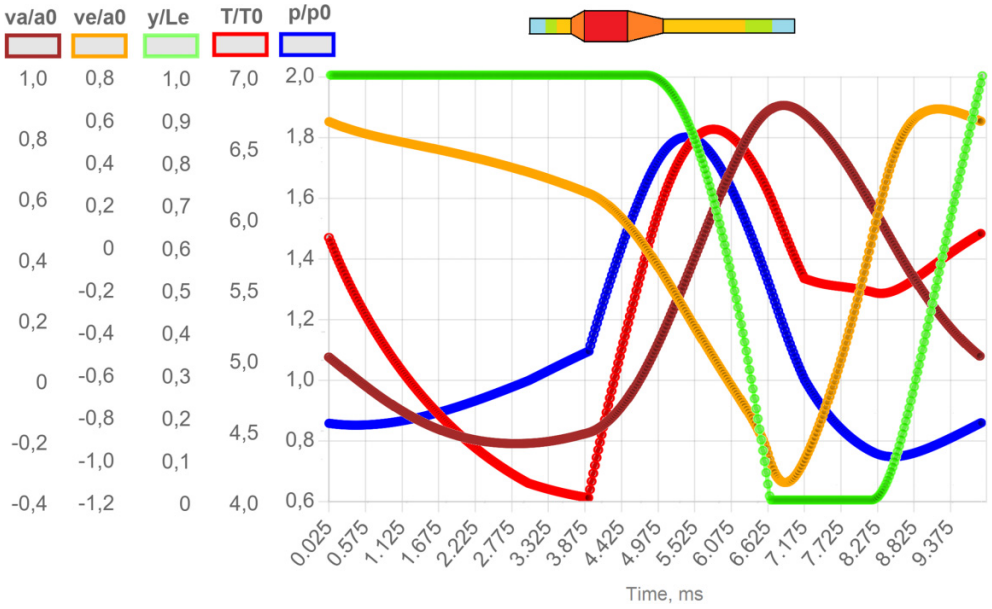

Fig. 20. Comparison of experimental instantaneous parameters with the results of simulation using the Pulsejet-Sim program (the simulation data are plotted on the experimental diagrams): (*a*) combustion chamber pressure and air flow for the Solar PJ32 engine (Litke et al. 2005); (*b*) combustion chamber pressure for the Argus As 014 engine (Manganiello et al. 1945*a*).

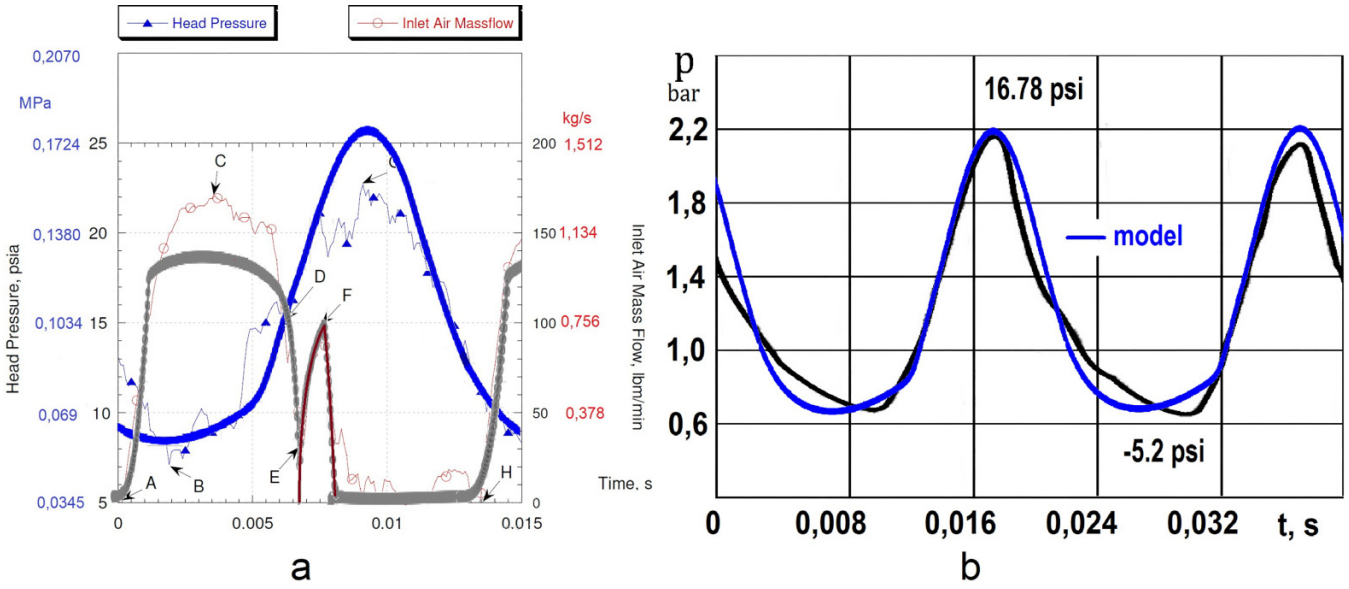

ulations without capital investments to their own HPC cluster.

For example, the program allows you to calculate parametric dependencies of parameters and diagrams over 300–500 calculation cycles of 2000 points each for several seconds (Fig. 17). To plot the diagrams, the method of smallest squares is used with the function of eliminating random errors exceeding the maximum permissible deviation.

Thus, Pulsejet-Sim demonstrates that the combination of the FOSS stack (Free & Open-Source Software) with a cloud architecture and a step-by-step GUI makes complex engineering simulations available as a service. The approach is easily scalable to related problems (internal combustion, detonation engines, pneumatic starting systems, and other systems with periodical workflow), where interactive selection of multiparameter models in real time is required.

Results and discussion

To assess the reliability of the proposed model and the efficiency of the Pulsejet-Sim program, calculations of the working process of various pulsy jet engines were performed (Figs.

Table 4. Comparison of the simulation results of the Argus As 109–014 and Solar PJ32 valved engines with experimental data (Manganiello et al. 1945*a*; Litke et al. 2005).

Engine	UAV	Purpose	Yearof development	Country	Parameter	Experiment	Model	Model error
Argus As 109–014	Fieseler Fi-103 (V-1)	Attack	1943	Germany	Thrust, N	2700–3000	2900	0.0
					Specific thrust, m/s	700–750	710	0.0
					Frequency, Hz	48–50	50	0.0
					Specific fuel consumption, kg/h*dN	3.2–3.6	3,3	0.0
Solar PJ32	KD2G-2 Firefly	Target	1951	USA	Thrust, N	450–500	450	0.0
					Specific thrust, m/s	700–800	735	0.0
					Frequency, Hz	70–80	76	0.0
					Specific fuel consumption, kg/h*dN	3.0	3.2	0.0

Fig. 21. Preliminary comparison of the simulation results for the Solar PJ32 engine with the available experimental data (Litke et al. 2005) (the axes have been reconstructed, the values in *N* have been added): (*a*) thrust and (*b*) specific thrust from fuel consumption.

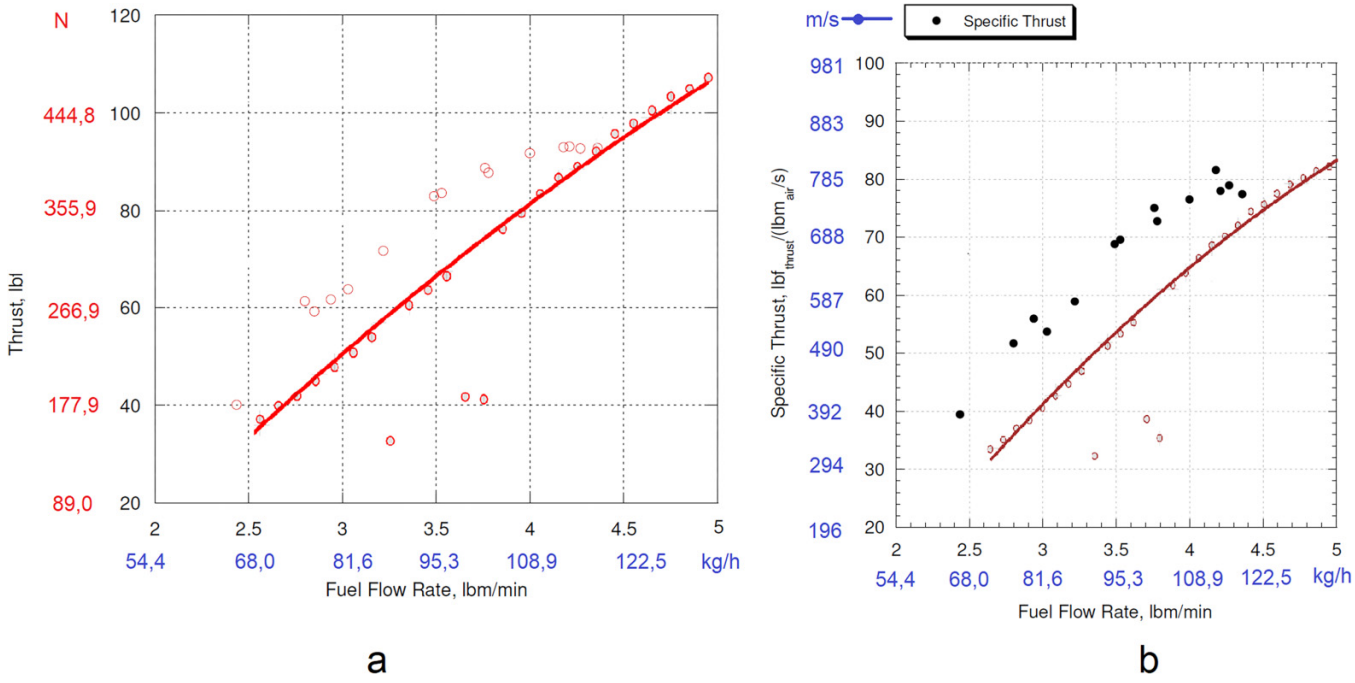

18 and 19), with subsequent comparison of the obtained results with experimental data.

The main problem with this comparison is that there are very little reliable data from real studies of pulsating engines. This is mainly due to the fact that a significant part of the pulsating engine projects after World War II were canceled as unpromising in favor of turbojet engines. After that, all subsequent developments were carried out mainly by private users, actually in garages, where there was no need for any real research. Therefore, except for the thrust force measured by a mechanical dynamometer (!), such studies are unremarkable, and no other data, with rare exceptions, were actually obtained. On the other hand, as already noted above, many scientific papers were not devoted to the study of engines for aircraft. All this makes the available data of little use for the purpose of validating the model and program.

At the same time, it should be noted that the results of tests of the valved Argus As 014 engine, conducted in the USA in the second half of the 1940s, are significantly more detailed. Despite the fact that the main results of such studies (Manganiello et al. 1945*a*; Valerino et al. 1946) were clearly obtained without the participation of the main German development specialists (Diedrich 1948; Gosslau 1957), they contain a significant amount of valuable information about the parameters and characteristics of this engine. In addition, it should be noted that the data from studies of scaled-down versions of the As 014 engine, in particular the serial Solar PJ32 engine for the KD2G-2 Firefly air target developed for the US Navy (Litke et al. 2005), are very useful, although these

Fig. 22. Preliminary comparison of the simulation results of the modeling the Argus As 014 enginethrust from the mixture composition at different flight speeds for the s with the available experimental data (Manganiello et al. 1945*a*; Valerino et al. 1946) (the have been reconstructed, the thrust values in *N* have been added).

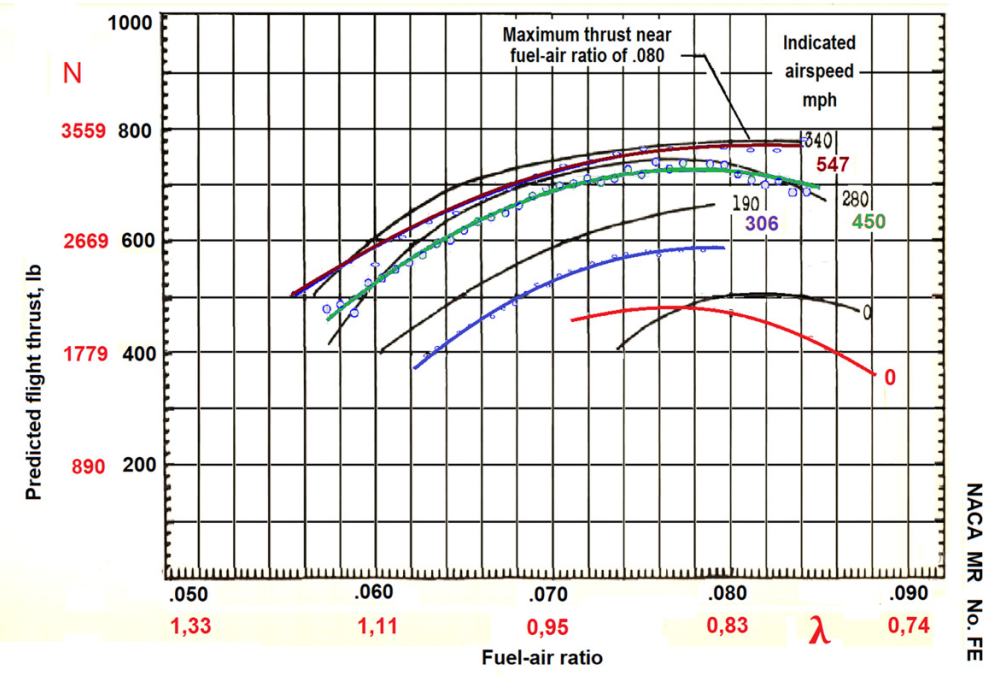

Fig. 23. Results of modeling the trajectory of the valve petal lifts with different petal thickness.

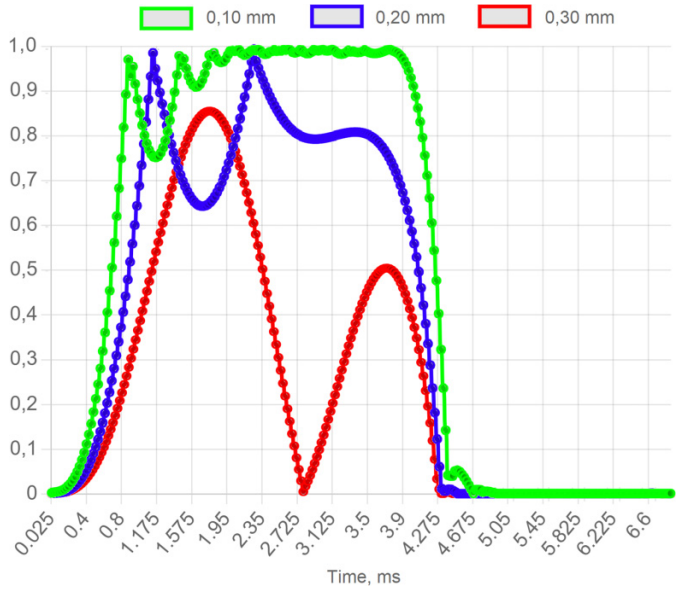

data contain some inconsistencies and require additional verification.

To preliminarily assess the model reliability, operation of these engines were simulated in a test bench conditions ($H = 0$, $v = 0$) for the fuel–air mixture composition $\lambda = 0.95$. The simulation results are presented in Fig. 20 and Table 4.

As follows from Table 1, the model in the considered range of sizes gives an error of less than 10% for all the main parameters of the engines.

The results of the comparison of the instantaneous pressure in the combustion chamber (Fig. 20) generally agree satisfactorily both qualitatively and quantitatively. The agreement for the instantaneous air flow rate (Fig. 20) is somewhat worse, which, with good agreement for other parameters, can be explained by the measurement error, possible erroneous processing and inaccurate interpretation of the measurement results.

Thus, when the petal bounces off the grate, the pressure in the chamber is already greater than the atmospheric one. But in the experimental diagram (Fig. 20), the air flow after closing the valves is incorrectly shown as positive (into the chamber). With a short intake channel, air flow into the chamber under such conditions is impossible, and a backflow of gases from the chamber must occur (negative instantaneous flow rate). Because of this, agreement is observed only if a similar section of the calculated flow rate curve with the opposite sign is applied to this section of the experimental diagram (marked in brown on the diagram).

In addition to these, a preliminary comparison was made of some characteristics of the Solar PJ32 (Fig. 21) and Argus As 014 (Fig. 22) engines obtained in Manganiello et al. (1945*a*), Valerino et al. (1946), Litke et al. (2005) with the simulation data, where it can be seen that, in general, the calculated curves are located quite close to the experimental ones.

At the same time, there is simply nothing to compare some of the results that the program produces with. For example, it was not possible to find reliable data on the instantaneous

Fig. 24. Parametric modeling the engine parameters depending on the petal thickness.

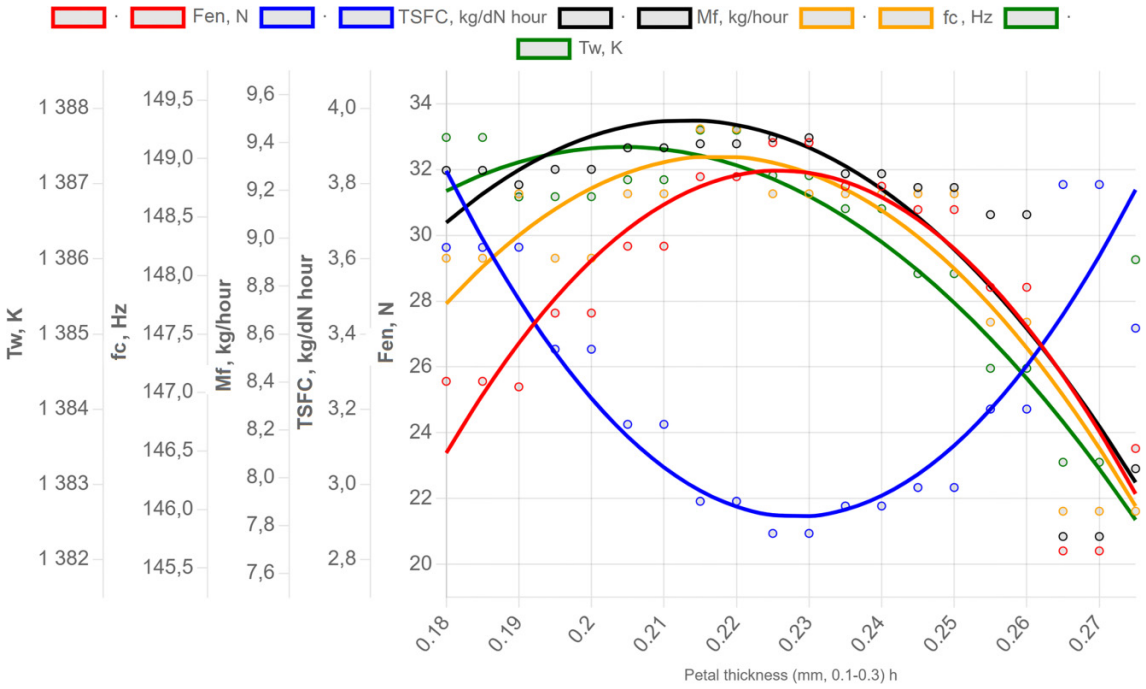

Fig. 25. Results of modeling the dependence of the main engine parameters on the length of the resonance pipe.

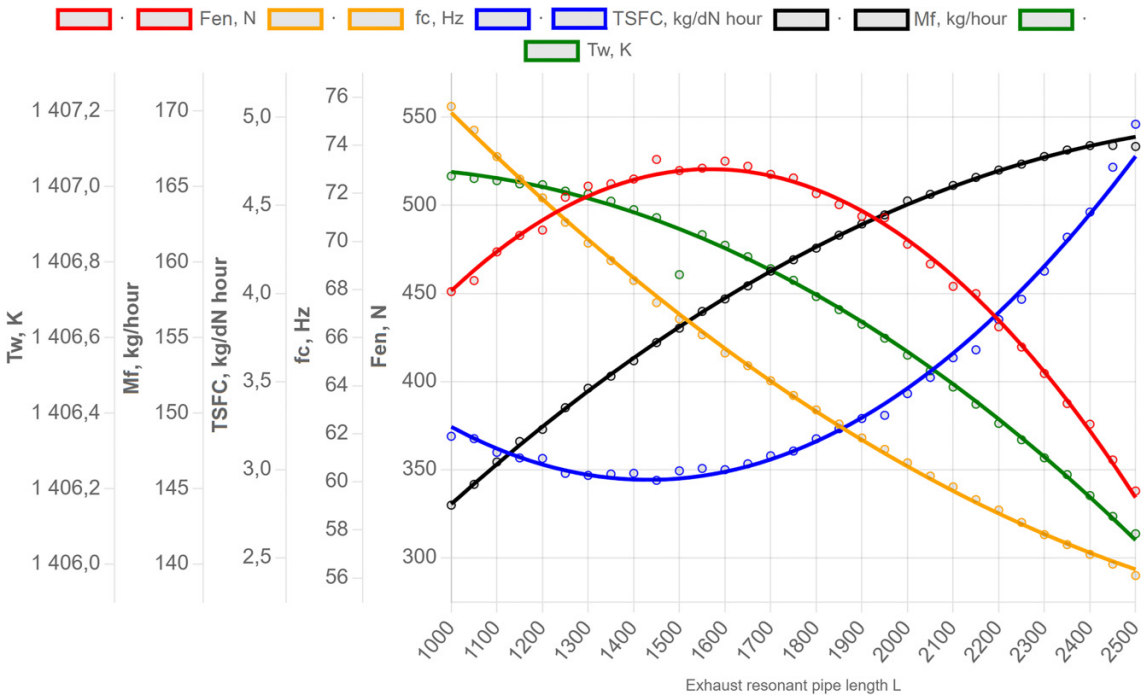

temperature measurement in the combustion chamber (Figs. 18 and 19), although the methods and equipment for such measurements have long been known. The same applies to gas velocity. There are also no reliable experimental data on the dynamics of the valve petal movement (Fig. 23), and especially on the influence of the petal parameters on the engine parameters (Fig. 24). In addition, the known sources do not contain even the most basic characteristics—for example, there are no data on the dependence of engine parameters on the length of the resonance pipe (Fig. 25) and the intake pipe (Fig. 26) in a valveless engine.

During the research, it was also noted that the valveless engine has a working process that is significantly different from the valved one. This is evident both from the diagrams of changes in instantaneous parameters in the cycle (Figs. 18 and 19). In addition, during the modeling, it was found that

Fig. 26. Results of parametric modeling of a small-sized valveless engine atdifferent length of the intake pipe.

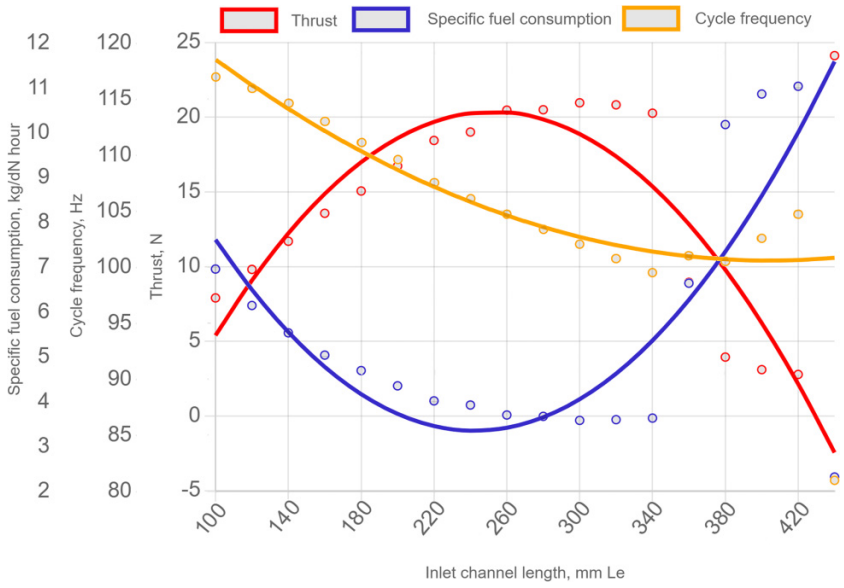

a simple intake pipe does not require devices to block the backflow of gases from the chamber through this pipe (similar to reed valves). Only the correct "adjustment" of the pipe dimensions is required, which also creates additional thrust when it flows out. Moreover, the Pulsejet-Sim program is currently the only tool that allows you to model both types of engines—both valved and valveless. However, so far only preliminary studies have been carried out, the results of which should be supplemented in the future.

It is worth noting separately the useful practical reaction of the Pulsejet-Sim program to the assignment of unrealistic or erroneous geometry. Usually such an engine does not start, that is, there is no self-oscillating process, and the parameter oscillations after 5–10 cycles after the starting one fade into a line. In case of a more serious error, the calculation stops with a corresponding warning to the user. Such properties increase the efficiency of using the Pulsejet-Sim program in practice.

Conclusions

1. The analysis of sources shows that there are currently no workable models and programs for simulating the working process and characteristics of pulse jet engines available to a wide range of users. On the one hand, this hinders the understanding of the working process of the pulse jet engine, and on the other hand, it complicates the correct selection of the engine type and the coordination of its characteristics with the UAV.
2. To create a program for modeling the parameters and characteristics of a pulsejet engine a universal thermodynamic model was developed to describe the instantaneous change in pressure and temperature, taking into accounts the mixing of flows, combustion and heat exchange in the combustion chamber of a pulse jet engine of valved and valveless types. Writing the equations describing the change in instantaneous gas parameters in dimensionless form also made it possible to find dimensionless criteria for the similarity of the pulse jet engine working process.
3. A universal model of air flow through a petal valve of various designs has been developed, taking into account dynamic phenomena, including inertia and elastic rebound of the petal from the valve grid and limiter.
4. Within the framework of the accepted assumptions of the "piston" analogy method, a model of non-stationary gas and air flow in the resonance tube of a pulse jet engine and in the intake pipe of a valveless engine has been developed. This ensured the universality of the model and, for the first time, made it possible to simulate two types of engines, both valved and valveless, within the framework of one model and program.
5. A special online Pulsejet-Sim program for simulating pulsejets has been developed for the first time, which is posted on a special website for access by a wide range of users. The program is implemented as a web-oriented software service built on a special data structure with division into server and client parts. As a result, in comparison with traditional desktop packages and applications, the online Pulsejet-Sim program does not require downloading to the user's computer and allows instant calculation using server resources with secure data storage in cloud storage. This makes Pulsejet-Sim an effective tool for both scientific laboratory researchers and UAV designers, as well as for students of educational courses.
6. Using the Pulsejet-Sim program, preliminary mathematical modeling of known samples of pulse jet engines was performed, which showed generally satisfactory qualitative and quantitative agreement with the available experimental data. Thus, a comparison of the calculated parameters of several valved-type pulse jet engines—thrust, specific fuel consumption, and cycle frequency, with experimental data shows that the model gives an error of less

than 10%. The results of modeling the instantaneous parameters of the cycle and some characteristics also give generally satisfactory quantitative and qualitative agreement with the available data.

7. Due to the lack of the necessary amount of experimental data it was not yet possible to conduct a full verification of the model and the program, including for the valveless engine; therefore, the obtained results should be supplemented in future studies. In addition, the research will also be continued in the direction of matching the characteristics of the pulse engine with the characteristics of the UAV and developing a corresponding model with the aim of including it in the Pulsejet-Sim program as an additional software service.

List of symbols

I	enthalpy, moment of inertia
Q	amount of heat
q	specific heat flux, specific load
p	pressure
T	temperature
v	velocity
ρ	density
m	mass
t	time
f	frequency
x, y	coordinate
V	volume
F	area, thrust, specific thrust
L, l	length
D, d	diameter
δ	thickness
b	width
E	modulus of elasticity
γ	heat capacity ratio
C_p	specific heat capacity at constant pressure
R	gas constant, thrust, force
M	Mach number, air, gas flow rate
Hu	fuel calorific value
η	combustion efficiency
μ	flow rate coefficient, dynamic viscosity
ξ	friction coefficient, hydraulic resistance
L_0	stoichiometric ratio
λ	air-fuel ratio, thermal conductivity
τ, π	gas dynamic functions
TSFC	specific fuel consumption
C_x	drag coefficient (The overbar over gas parameters indicates the dimensional values)

Acknowledgements

The authors like to express his gratitude to the AB-Engineering Mechanical Processing Center, Odesa, and the International Motor Bureau, Nemishaieve settlement, Kyiv oblast, Ukraine, for technical support, including for providing materials and technical data of different engines, as well as for help in the research.

Article information

History dates

Received: 14 May 2025
Accepted: 16 December 2025
Accepted manuscript online: 24 December 2025
Version of record online: 5 February 2026

Copyright

Data availability

Data generated or analyzed during this study are provided in full within the published article.

Author information

Author ORCIDs

Alexander Khrulev https://orcid.org/0000-0002-6841-9225

Author contributions

Conceptualization: AK, VM
Data curation: AK, VM
Formal analysis: AK
Investigation: AK
Methodology: AK, VM
Project administration: AK
Resources: AK
Software: VM
Supervision: AK
Validation: VM
Visualization: VM
Writing – original draft: VM, AK
Writing – review & editing: AK

Competing interests

The authors declare no competing interests.

Funding information

This study was not supported by any grants from funding bodies in the public, private, or not-for-profit sectors.

References

Agarwal, A., and Pitso, I. 2020. Modelling & numerical exploration of pulsejet engine using eddy dissipation combustion model. Mater. Today: Proc. **27**: 1341–1349. doi:10.1016/j.matpr.2020.02.620.

Ahmadian, S. Computational approach in sizing of pulsejet engine. Emirates University, January 2014. 25. Available from https://www.researchgate.net/publication/284511823 [accessed date 5 May 2025]

Anand, V., Jodele, J., Prisell, E., Lyrsell, O., and Gutmark, E. 2020. Dynamic Features of Internal and External Flowfields of Pulsejet Engines. AIAA J. **58**(10): 4204–4211. doi:10.2514/1.j059685.

Anand, V., Jodele, J., Shaw, V., Russell, A., Prisell, E., Lyrsell, O., and Gutmark, E. 2019a. Visualization of valved pulsejet combustors and evidence of compression ignition. Flow Turbul. Combust. **106**(3): 901–924. doi:10.1007/s10494-020-00203-4.

Anand, V., Jodele, J., Zakh, A., Geller, A., Prisell, E., Lyrsell, O., and Gutmark, E. 2019b. Revisiting the Argus pulsejet engine of V-1 buzz bombs: an experimental investigation of the first mass-produced pressure gain combustion device. Exp. Therm Fluid Sci. **109**: 109910. doi:10.1016/j.expthermflusci.2019.109910.

Arpaci, V.S., Dec, J.E., and Keller, J.O. 1993. Heat Transfer in Pulse Combustor Tailpipes. Combust. Sci. Technol. **94**(1–6): 131–146. doi:10.1080/00102209308935307.

Babu, V. 2015. Fundamentals of gas dynamics. 2nd ed. John Wiley & Sons Ltd, Chichester, 262.

Biringen, S., and Chow, C. 2011. An introduction to computational fluid mechanics by example. John Wiley & Sons, Inc. doi:10.1002/9780470549162.

Bootstrap: the most popular HTML, CSS and JS library in the World. Available from https://getbootstrap.com/ [accessed date 5 May 2025]

Cavcar, M. The International Standard Atmosphere (ISA). **7**. Available from http://fisicaatmo.at.fcen.uba.ar/practicas/ISAweb.pdf [accessed 5 May 2025]

Ceviz, M.A., and Kaymaz, I. 2005. Temperature and air–fuel ratio dependent specific heat ratio functions for lean burned and unburned mixture. Energy Convers. Manage. **46**: 2387–2404. Available from https://www.researchgate.net/publication/222535464 [accessed 5 May 2025]. doi:10.1016/j.enconman.2004.12.009.

Clark, C., and Kimmons, R. 2023. Cognitive load theory. EdThechnica. doi:10.59668/371.12980.

Diedrich, G. 1948. The Aero-Resonator Power Plant of the V-l Flying Bomb. Project SQUID. Princeton, New Jersey, 46.

GasTurb 14. 2023. Design and Off-Design Performance of Gas Turbines. GasTurb GmbH. 379. Available from https://gasturb.com/Downloads/Manuals/GasTurb14.pdf [accessed date 5 May 2025]

Glassman, I. A., and Yetter, R.A. 2008. Combustion. 4th ed. Academic Press, Burlington, 794.

Globe Corporation XKD5G-1 Target Drone. National Air and Space Museum. Steven F. Udvar-Hazy Center in Chantilly, VA. Available from https://airandspace.si.edu/collection-objects/drone-target-xkd5g-1/nasm_A19660166000 [accessed date 5 May 2025]

Gonzalez, I., Naseri, A., Rigola, J., Perez-Segarra, C.D., and Oliva, A. 2017. A fluid-structure interaction solver for the fluid flow through reed type valves. 10th International Conference on Compressors and their Systems. IOP Conf. Series: Materials Science and Engineering. **232**: 012032. 11p. doi:10.1088/1757-899X/232/1/012032.

Gosslau, F. 1957. Development of the V-1 pulse jet. A History of German Guided Missiles Development /*Edited by* Th.Benecke and A.W.Quick. First Guided Missiles Seminar. Munich Germany, April, 1956 / Brunswick, Germany, 400–418.

Guha, A. 2001. An efficient generic method for calculating the properties of combustion products. Proc Instn Mech Engrs (IMechE), **Vol 215**, Part A, 375–386. Available from http://www.facweb.iitkgp.ac.in/~aguha/research/IMechE2001-combustion.pdf [accessed date 5 May 2025]

Hoerner, S.F. 1992. Fluid-Dynamic Drag. Practical Information on Aerodynamic Drag and Hydrodynamic Resistance: theoretical, experimental and statistical information. Library on Congress Catalog Card Number 64-19666, 455.

Idelchik, I.E. 1966. Handbook of hydraulic resistance. Coefficients of local resistance and of friction. New York: Israel Program for Scientific Translations Ltd., 517.

Isac, J.K.R., Mohanraj, L., Sai, E.S., and Kannan, V.K. 2014. Numerical simulation of a hydrocarbon fuelled valveless pulsejet. Propuls. Power Res., **3**(2): 90–95. doi:10.1016/j.jppr.2014.05.004

Jenkins. Build great things at any scale. Availabe from https://www.jenkins.io/ [accessed date 5 May 2025]

jQuery. Available from https://jquery.com/ [accessed date 5 May 2025]

Khrulev, A, Saraiev, O, Saraieva, I, and Vorobiov, O. 2024. Modeling of thermodynamic processes in internal combustion engine cylinder during cranking in compression measurement tests. Combustion Engines, **198**(1): 3–14. doi:10.19206/CE-187380.

Khrulev, A. 2023a. Determination of gas parameters in resonant pipes and channels of engines with a periodic workflow using the piston analogy method. Eastern Eur. J. Enterp. Technol. **5**(7 (125)): 50–59. doi:10.15587/1729-4061.2023.288520.

Khrulev, A. 2023b. Mathematical modeling of reed valve operation in engines with periodic workflow. Integration of science as a mechanism of effective development: Proceeding of the 11th International scientific and practical conference, November 28 - December 01, 2023, Helsinki, Finland/International Science Group, Helsinki, P. 389–395.

Khrulev, A. 2024. Modeling work-flow of the "cylinder-piston" type devices using a universal thermodinamic model. Evol. Mech. Eng. **5**(4): EME.000618. doi:10.31031/EME.2024.05.000618.

Khrulev, A.E., and Saraev, O.V. 2021. The method of expert assessment of the technical condition of an automobile engine after overheating. Automob. Transp. **48**: 5–16. doi:10.30977/AT.2219-8342.2021.48.0.5.

Kravchenko, O., Khrulev, A., Gerlici, J., Saraiev, O., and Danets, S. 2024. Technical condition assessment and modelling of reed valves in vehicle engine intake systems. Commun. Mech. Eng. Transp. **27**(1): B41–B52. doi:10.26552/com.C.2025.006.

Lienhard-IV, J.H., and Lienhard-V, J.H. 2008. A heat transfer textbook. 3rd ed. Phlogiston Press, Cambridge, MA, 750.

Litke, P.J., Schauer, F.R., Paxson, D.E., Bradley, R.P., John, L., and Hoke, J.L. 2005. Assessment of the performance of a pulsejet and comparison with a pulsed-detonation engine. 43rd AIAA Aerospace Sciences Meeting and Exhibit. January 10-13, Reno, Nevada, 10. doi:10.2514/6.2005-228.

Lockwood, R.M. 1963. Hiller Pulse Reactor Lift Engine. Final Report. Advanced research. Report NO. ARD 308. Bureau of Naval Weapons. Propulsion Dept. Contract NOw 61-0226-c. 230p.

Manganiello, E.J., Michael, F., Valerlino, M.F., and Essig, R.H. 1945a. Sea-level performance tests of a 22-inch -diameter pulse-jet engine at various simulated ram pressures. Aircraft Engine Research Laboratory. Cleveland, Ohio. Memorandum Report E5J02, NACA, Washington, 39.

Manganiello, E.J., Valerino, M.F., and Breisch, J.H. 1945b. Endurance tests of a 22-inch-diameter pulse-jet engine with a neoprene-coated valve grid. NACA Memorandum Report E5J03. Aircraft Engine Research Laboratory, Cleveland, Ohio, 15.

Meng, X., de, Jong W., and Kudra, T. 2015. A state-of-the-art review of pulse combustion: Principles, modeling, applications and R&D issues. Renew. Sustain. Energy Rev. 42. doi:10.1016/j.rser.2015.10.110.

Migalin, K.V., Ambrozhevich, A.V., Sereda, V.A., Larkov, S.N., Boychuk, I.P., Kartashev, A.S., and Silevich, V.Yu. 2014. Pulsejet air-breathing engines: monograph. Under the gen. *Edited by* K.V. Migalin. Tolyatti, TSU Publ. House, 296(on Russian)

Mittal, V. 2025. The Novel Pulse Jet Engine Powering The Ukrainian Trembita Missile. Forbes, Jan 13. Available from https://www.forbes.com/sites/vikrammittal/2025/01/13/the-novel-pulse-jet-engine-powering-the-ukrainian-trembita-missile/ [accessed date 5 May 2025]

Mohsen, K.K., and Hussain, Z.H. 2021. Numerical comparison between two tailpipe shapes of valved pulsejet engine. INTCSET 2020. IOP Conf. Series: Materials Science and Engineering **1094**: 012001. 13. doi:10.1088/1757-899X/1094/1/012001.

Newdick, T. 2024. Pulsejet Drone Flies, Could Have Big Impact On Cost Of Future Weapons. The War Zone, Mar 6.Available from https://www.twz.com/news-features/pulsejet-drone-flies-could-have-big-impact-on-cost-of-future-weapons [accessed date 5 May 2025]

Pearson, R. J., Bassett, M. D., Fleming, N. P., and Rodemann, T. 2002. Lotus Engineering Software—an approach to model-based design. The 2002 North American ADAMS Conference in Scottsdale. Arizona. Available from https://ru.scribd.com/document/215011237/Lotus-Paper [accessed date 5 May 2025]

Pisarenko, G.S., Kvitka, O.L., and Umansky, E.C. 2004. Streight of Materials. 2 ed. Kyiv, Vyscha Shk., 655 (on Ukrainian)

Prisacariu, V. 2022. Performance analysis of military flying wing uav with pulse jet engine. Review of the Air Force Academy No.**2**(46): 36–47. doi:10.19062/1842-9238.2022.20.2.4.

Pulsejet-Sim: Pulsejet Engine Workflow Simulation Program. Available from https://pulsejet-sim.com [accessed date 5 May 2025]

Pydantic. Documentation for version: v2.11.4. Available from https://docs.pydantic.dev/ [accessed 5 May 2025]

Rohsenow, W.M., Hartnett, J.P., and Cho, Y.I. 1998. Handbook of heat transfer. 3rd ed. New York, McGraw-Hill, 1500.

Rolls-Royce. 1996. The jet engines. 5th ed. Rolls-Royce plc, Birmingham, 278.

Sánchez, A.A. 2022. Design, construction and testing of a Pulsejet engine (versão final após defesa). Dissertação para obtenção do Grau de Mestre em Engenharia Aeronáutica (2° ciclo de estudos). Covilhã, 87.

Schetinkov, E.S. 1965. Physics of Gas Combustion. Publishing House "Nauka," Moscow, **744**(on Russian)

Schmidt, P. 1957. On the history of the development of the Schmidtrohr. A history of german guided missiles development. *Edited by* Th. Benecke and A.W. Quick. First Guided Missiles Seminar. Munich Germany, April, 1956/ Brunswick, Germany, 375–399.

Shultz-Grunow, F. 1947. Gas-dynamic investigations of the pulse-jet tube. Parts I and II. National Advisory Committee for Aeronautics. Technical Memorandum No. 1131. Technical High School, Aachen, Germany. NACA, Washington, 112.

Simpson, B. 2004. The Enthusiast's Guide to Pulsejet Engines. 106. Available from https://www.academia.edu/28974608/Pjbookrev2a [accessed date 5 May 2025]

Tegné, J. 2022. Analysis of the operation of the pulsejet engine. 33rd Congress of the International Council of the Aeronautical Sciences. Stockholm, Sweden, 4–9 September, 2022/Stockholm, 24. Available from https://www.icas.org/icas_archive/ICAS2022/data/papers/ICAS2022_0120_paper.pdf [accessed date 5 May 2025]

Valerino, M.F., Essig, R.H., and Hughes, R.F. 1946. The effect of increase in combustion-air inlet temperature from 80° to 130° F on the sea-level performance of a 22-inch-diameter pulse-jet engine. Aircraft Engine Research Laboratory. Cleveland, Ohio. Memorandum Report E6G01, NACA, Washington, 19.

Van Heerbeek, P. A. 2008. Mathematical modelling of a pulse combustor of the helmholtz-type. Delft, **146**. Available from https://diamhomes.ewi.tudelft.nl/~kvuik/numanal/heerbeek_afst.pdf [accessed date 5 May 2025]

Wave Engine Corp. URL: Available from https://wave-engine.com/ [accessed date 5 May 2025]

Werzner, E., Ray, S., and Trimis, D. 2010. Turbulent pulsating flow through circular ducts. Proceedings of the 37th National & 4th International Conference on Fluid Mechanics and Fluid Power. FMFP10 - AM - 07. December 16–18, 2010, IIT Madras, Chennai, India /Madras, 7. Available from https://www.semanticscholar.org/paper/Turbulent-Pulsating-Flow-Through-Circular-Ducts-Werzner-Ray/a4316637d54239030a24cf55a58300d07349363a [accessed date 5 May 2025]

Wikipedia. 2025a. Continuous integration. Available from https://en.wikipedia.org/wiki/Continuous_integration [accessed date 5 May 2025].

Wikipedia. 2025b. Method of characteristics. Available from https://en.wikipedia.org/wiki/Method_of_characteristics [accessed date 5 May 2025].

Wikipedia. 2025c. Trembita (cruise missile). Available from https://en.wikipedia.org/wiki/Trembita_(cruise_missile) [accessed date 5 May 2025].